Studies on Passive, Carbon Nanotube RFID Systems and Applications with Consideration of Anti-Collision MAC

A Thesis Submitted to the Department of Computer Science and Communications Engineering,
the Graduate School of Fundamental Science and Engineering of Waseda University
in Partial Fulfillment of the Requirements for the Degree of Master of Engineering.

Submission Date: July 18th, 2022

Gentaro KONISHI
(5120FG26-5)
Advisor: Prof. Shigeru SHIMAMOTO
Research guidance: Research on Wireless Network Systems

Abstract

Whilst optical identification methods, such as barcodes and quick response (QR) codes had transformative impacts across multiple industries, radio frequency identification (RFID) has brought promise to a variety of smart applications for the successive generation of inventory management. Despite their characteristic advantages, RFID tag integrated circuits (ICs) are typically made of Silicon, which are expensive to manufacture. Research bodies across the globe have thus adopted a print-like roll-to-roll process, with which state-of-the-art innovations have been achieved.

In response to such recent innovations, three areas of interest have been investigated in this thesis: electromagnetic analysis of multiple access scenarios (Chapter 4), field programmable logic device (FPGA) implementation of anti-collision schemes (Chapter 5) and lastly, an application specific method for hybrid access in RFID-based smart refrigerators (Chapter 6). The findings from each investigation have been used to determine the experimental plans and future considerations for realizing novel anti-collision schemes to be employed with the next generation of RFID tags.

The analysis of simplified multiple access scenarios was investigated for the variability of different multiplexing domains, viz, code, power, frequency and time. Simulations sufficiently indicate that code and power domains are most suitable for anti-collision in RFID systems, due to the high variability of spectral and temporal dimensions. Consequently, a code domain anti-collision implementation has been conceptualized, where in which a universal asynchronous receiver and transmitter (UART) base program was considered as the transmission backbone. Despite the advantages of system simplicity, it was determined that the code domain concept required further consideration of impedance matching and the implementation of a reader, in order to obtain reliable testing results in the future. A power domain anti-collision method has also been proposed, which relies on application specific characteristics of refrigerators, namely, the power attenuation through dielectric shelves. The preliminary observations showed that indeed, the shelves inside refrigerators provide power attenuation for producing greater power level differences. However, further investigation is required for assessing the effects on bit-error-rate (BER) performance. Although the consideration of anti-collision in RFID systems is challenging due to the high variability of the channel, the consideration of application-specific features is likely to assist in successful realization of novel schemes.

Acknowledgements

I would like to thank my primary supervisor and professor, Shigeru Shimamoto for his invaluable guidance throughout my graduate program. Your advice and sharing of experiences have been enlightening and has greatly contributed to the success of my academic milestones in the 2 years, leading up to the writing of this thesis.

I would also like to express my sincere appreciation towards supervisor and lecturer, Megumi Saito, for her support in both academic and non-academic areas of my career as a graduate student. Your feedback and overwhelming patience, as well as your expressive determination towards the betterment of academic life for students has, without a doubt, contributed to the positive experience I had during my degree. Thank you.

I would also like to extend my thanks to laboratory leader and PhD Candidate, Kazutoshi Yoshii, for constantly being the friendly face, with who I was always able to share and discuss any concerns and questions I had throughout the program.

Thank you to the laboratory staff members as well as my fellow colleagues for making my master's degree an enjoyable experience. I have also learned a lot about the local culture (Japan) through you all, so thank you.

Finally, I would like to thank my family and friends for their unparalleled support. I simply could not have done this without you. Thank you.

Gentaro Konishi

July 2022

To my parents, for their unparalleled support and enabling this opportunity.

Table of Contents

Table of Figures

Chapter 1

Introduction

Identification technologies contributed to the unparalleled expansion of logistics and retail industries. Such technologies have also gained attention in recent years as promising components towards achieving smart cities in the future.

Optical barcodes and quick response (QR) codes have been adopted by nearly all industries with a plethora of use cases, including social media networking, logistic supply chains, retail sectors and public advertisement displays [1], [2]. Despite their rather ubiquitous nature, optical identification methods fall short in supporting increased volume of items in need of tracking and identification. Furthermore, optical codes require line-of-sight (LOS) operation, which consequently demands greater manual labor by an operator.

Meanwhile, radio frequency identification (RFID) has yet to grow into a multi-industry staple in inventory management, internet of things (IoT) and smart applications. Unlike barcodes and QR codes, RFID systems operate on a wide range of radio frequencies. RFID systems are thus able to exploit the non-line-of-sight (NLOS) and long-range operative advantages of radio frequency devices – which are desirable characteristics, particularly in the identification regime.

Despite their attractive advantages and operating characteristics, RFID systems also have their own disadvantages. Currently, a typical RFID tag consist of a Silicon-based semiconductor integrated circuit (IC). Such ICs require numerous chemical processes and are expensive to manufacture, and costs have suffered further inflation due to the recent Silicon shortage [3].

In response to the Silicon-related challenges, research bodies across the globe have been investigating alternative manufacturing methods. Specifically, an alternative method that has gained attention in semiconductor manufacturing is the roll-to-roll process. This process effectively adopts a printing process, via layer lamination. Furthermore, carbon-nanotube composites have also been utilized as the key material for semiconductors, such as in the case of the recent innovations by Toray Industries, Inc [4].

This thesis details the analyses and system proposals in relation to RFID systems, as well as anti-collision methods (multiple access schemes) for concurrent identification. An analysis of multiple access scenarios, anti-collision implementation in field programmable logic devices (FPGAs) and application specific RFID systems are investigated in this work. All three areas of work aim to develop an anti-collision method for RFID systems via simulations and in the future, practical experiments. Discussions are based upon the perspectives of electromagnetics, electronics, embedded systems and wireless communication.

Chapter 2 provides as overview of existing identification technologies, followed by the elaboration of a new, state-of-the-art RFID tag IC in Chapter 3. Multiple access scenarios and their analyses in full-wave simulation are presented in Chapter 4, followed by the conceptualization of a UART-CDMA based anti-collision scheme and the discussion of its future implementation in Chapter 5. An application specific anti-collision method for smart refrigerators is proposed in Chapter 6, as well as its future challenges and implications ahead of system realization. Lastly, the conclusions of this thesis (primarily Chapters 4, 5 and 6) are provided in Chapter 7.

Chapter 2

Overview of Identification Technologies

2.1 Identification Technologies

Current identification technologies primarily include Quick Response (QR) codes, barcodes and Radio Frequency Identification (RFID). All systems have respective advantages and disadvantages. Identification technologies transformed the communications, logistics and retail industries and almost all materials and items across the supply chain are tagged with some form of identification device. This chapter provides a high-level overview of three identification technologies, the barcode, QR code and RFID. The subsection on RFIDs have been more closely investigated due to its considerable relevance to the contents of this thesis as a w hole.

2.2 Barcodes

Barcodes, invented by Norman J. Woodland and Bernard Silver in 1948 originated from the visualisation of Morse Code. The basic structure of barcodes consists of thickness varying stripes that are distributed in one dimension.

The objective, which resulted in this outstanding invention, was to simplify and streamline checkouts at supermarkets and inventory management in general. The original form of barcodes was very large due to the analogous nature of electronics back when the technology was first invented, and the physical size of barcode readers were known be comparable to that of refrigerators [2], [6].

In more recent times, barcodes are often inkjet printed in very compact form on paper and are found in almost every item in a supermarket, as well as many other retail environments. A diagrammatic representation of a modern barcode is shown in Fig. 1.

Barcodes are incredibly inexpensive to produce and simple to design. As they are often printed on thin materials, there is little to no addition in product volume or weight, which is advantageous in distribution scenarios where transport costs are certainly non-negligible.

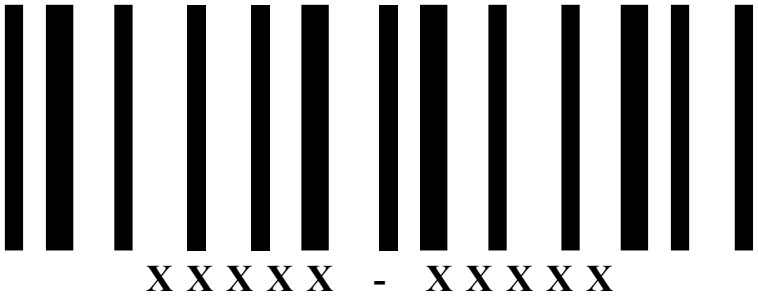

Figure 1. Diagrammatic representation of a modern barcode.

2.3 Quick Response Codes

The barcode was a technology widespread across multiple industries due to its numerous benefits to productivity. However, before the beginning of the 20th century, manufacturing and the scale of production changed, and demanded an increase in code capacity. Barcodes are known to store around 20 alphanumeric characters [1] which, due to the ever-increasing production sophistication and volume across industries, were deemed insufficient – leading to time and financial inefficiency.

In response to the shortcomings of the one-dimensional predecessor, Masahiro Hara a lead engineer who works for Denso-Wave, Japan, along with one other engineer, came up with a two-dimensional, matrix form variant of the barcode: the QR (Quick Response) Code [1]. As shown in Fig. 2 (a diagrammatic representation), the QR code consists of three position detection patterns located at three corners of the square form factor. The detection patterns assist in providing improved accuracy, preventing false detection and robustness to various read angles.

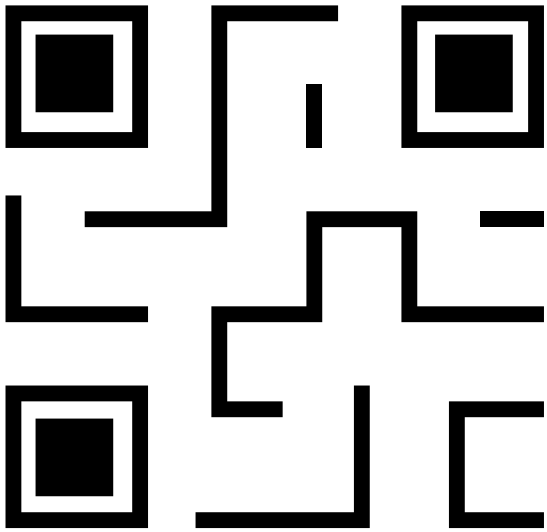

Figure 2. Diagrammatic representation of a QR Code.

Due to the two-dimensional nature of QR codes, supplemented by various innovations towards high accuracy and robustness against real-world challenges, this code variant is said to be faster (more responsive) than the original barcode by a factor of ten. In addition, the storage capacity of alphanumeric characters has been demonstrated to be in the order of several thousand [1]. In short, QR codes are a higher capacity successor of barcodes with added advantages in addition to those attributed to barcodes.

2.3.1 Shortcomings Optical Methods

QR codes and barcodes each have their own advantages. However, given the immensely large inventory volumes in applicable situations (distribution, retail), such codes also have disadvantages that will, in the near future, impede the expansion and efficiency of large-scale inventory management in smart cities and smart logistics. The primary disadvantage is the need for a user (or machine) to scan the code on each item, one at a time – limiting productivity. This disadvantage has two underlying issues: this identification methods requires considerable assistance by a human being and the barcodes cannot be read with any degree of concurrency. Another disadvantage is that both the barcode and QR codes require optical line-of-sight (LOS) conditions for proper operation. This can be challenging in situations where items a stacked in an unorganised manner such that the codes are hidden from sight.

2.4 Radio Frequency Identification (RFID)

With the steady increase in the demand for automation, efficiency and volumetric capacity in logistic and retail environments, RFID-based systems have been the research of focus due to their numerous advantages over aforementioned optical code technologies.

A typical RFID system consists of a reader (the interrogator) and a tag (with stored information). Between the two devices is a wireless channel through which the forward link and reverse link signals are exchanged. A diagrammatic description of a typical RFID system is shown in Fig. 3.

The reader would first transmit an interrogation signal towards the vicinity of the tag, with which (for a passive tag) the tag would harvest the energy from received signal to power the tag IC (integrated circuit) and re-transmit signals of stored data via what is often referred to as backscatter modulation.

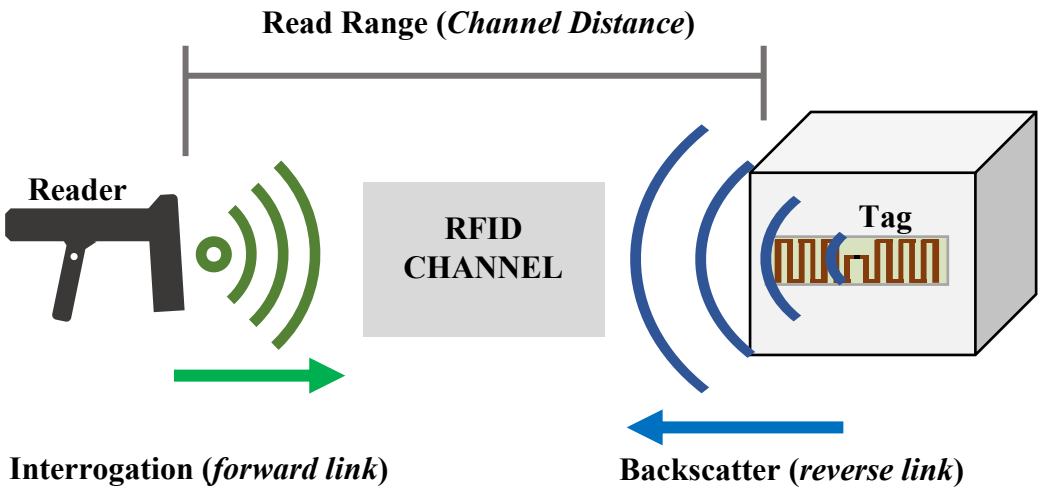

Figure 3. Channel diagram of an RFID system.

2.4.1 RFID Multiple Access

In RFID multiple access, not one, but several tags are interrogated by the reader at the same time. Naturally, as with any other multiple access channel in wireless communications, overlapping signals arriving at the reader (via multiple backscatter paths), packet collisions at the reader occur. Time Domain methods such as ALOHA have been widely used as the collision method for existing RFID systems. However, there is still a need to develop better performing (lower BER) anti-collision methods through the incorporation of CDMA, NOMA and other innovative multiplexing methods.

2.4.2 RFID Power Source and Operating Frequencies

RFID systems can consist of passive, semi-passive and active tags or various geometries that operate in LF (Low-Frequency), MF (Medium-Frequency), HF (High-Frequency), UHF (Ultra-High-Frequency) and higher, microwave frequencies.

Power Source: A passive RFID tags are powered solely via energy harvested from the interrogation (forward link) signal transmitted by the reader. Currents induced in the antenna are used to power both the tag IC (integrated circuit) as well as the reverse link backscatter. Active tags are (typically) powered by their own batteries, i.e., both their antenna and their IC. Active tags generally offer greater read range because of their power capabilities in return for greater cost of purchase. Semi-active tags, as the name suggests, are only partially powered by their own battery. With semi-active tags, the tag IC is powered by a battery, whilst the antenna is powered by via energy harvesting to allow for backscatter transmission [6].

Operating Frequencies: LF, MH, HF, UHF and upper microwave frequencies are all used for RFID applications. Intuitively, higher frequencies allow for greater bandwidth which can be useful for larger volumes of information stored in each tag. The read range of an RFID channel is also known to be practically dependant on the operating frequencies as well. Specifically, RFIDs operating in the UHF band are known to have read ranges of over 10 meters with passive tags, or even over 100 meters with the use of active tags. On the other hand, HF operated tags are known to support channel distances of up to 1 meter [7].

2.4.3 Advantages and Disadvantages

Since RFID systems operate with radio frequencies and enable NLOS operation, such systems offer an attractive support for concurrent identification. That is, unlike the optical codes such as barcodes and QR codes mentioned in Section 2.2 and 2.3, data from multiple tags can be obtained in a very short amount of time via the use of packet anti-collision techniques that are widely used in cellular mobile communication.

The combination of multiple access (via anti-collision techniques), NLOS detection and long-range UHF operation, RFID systems would facilitate inventory monitoring within retail environments as well as entire supply chains from production to distribution in an efficient manner. Furthermore, data stored in RFID tags can be re-written which could contribute to cost savings from a long-term perspective.

The most common material used for manufacturing RFID tag ICs is Silicon. Due to the reliable manufacturing of Silicon-based ICs, RFID tags that are based on Silicon have the benefit of long-term operation and high (charge) carrier mobility which enables the support for higher operating frequencies. This is in addition to the advantages outlined earlier in this chapter.

Despite the benefits of supporting concurrent identification and larger data transmission, Silicon-based RFIDs are expensive to manufacture, relative to QR codes and barcodes. Silicon integrated circuits (ICs) demand a huge number of chemical processes and the use of costly equipment, which takes away from the functional and performance benefits of RFID systems. A good example of this disadvantage is the use of expensive Silicon-based RFIDs for low-value retail goods, i.e., the cost of production of such RFIDs would be large comparison to the financial value of the sold item that has the tag attached. These disadvantages encouraged numerous research bodies to investigate the development of low-cost RFID tag ICs.

2.5 Summary

The one-dimensional optical code based on the Morse code dramatically streamline the retail industry, before quickly spreading to many other industries including logistics and distribution. The QR code was a two-dimensional successor of the barcode, adding far greater data capacity as well as high speed pattern detection. Whilst the optical codes are low-cost and come with a number of benefits, their shortcomings are becoming more apparent. Substantial increases in volume and demand for efficiency in inventory management have oriented researchers and industry towards a superior alternative: RFID technology. RFID systems certainly have their own disadvantages but are far outweighed by the benefits they could bring to industries that optical methods otherwise could not.

Chapter 3

A Low-Cost Alternative to Silicon Tag IC

3.1 Carbon Nanotube Composite-based Semiconductor

The financial disadvantages Silicon-based RFIDs as described in Section 2 have encouraged new studies which have been conducted around the globe for the development of RFID tags fabricated using coating or a Roll-to-Roll (R2R) process.

An R2R process, in the production of RFID tags, involves the propagation of a sheet of flexible tag dielectric (such as PVC) through multiple stages of 'rolls,' or rotating cylinders. Through each roll stage, the final device (the tag) is gradually laminated onto the dielectric with which, in the end, results in what is effectively a printed tag.

Using this R2R process, groups across the world have been able to develop low-cost alternatives to the silicon gold standard of ICs. Those in Japan, Norway and the UK have developed printed oxide semiconductors with carrier mobilities of up to $50cm^2V^{-1}$. Despite this impressive feat, the carrier mobilities achieved by such entities are still limiting in performance. This is because the carrier mobility of semiconductors determines the maximum allowable operating frequency of printed ICs. Specifically, the tags ICs with $50cm^2V^{-1}$ carrier mobility semiconductors are only capable of operating in the High Frequency (HF) band which further limits their effective communication ranges to under 50cm in RFID systems.

Meanwhile, Toray Industries claimed to have achieve the world's first printed RFID tag incorporating a Carbon nanotube (CNT) composite-based chip [4], [8] with a world-record carrier mobility of $182cm^2\,V^{-1}$, printed via low-cost roll-to-roll (R2R) process. Through the use of the unique physical properties of carbon nanotubes uniquely combined with a polymer material, Toray has been able produce a semiconductor with over three-fold carrier mobility compared to the oxide-based competitors. The emergence of this low-cost, high performing solution for UHF RFID fabrication offered encouraging prospects for the distribution of low-cost RFID tags, particularly in the logistics and retail industries.

3.2 Joint Research

Toray Industries, Inc. is a Japanese company with globally expanded offices that focuses on the development and manufacturing of basic materials [9], [10]. Materials include fibers, polymers and various chemicals. Production has also been expanded to electronics and IT-related sectors.

Upon their recent break-through development (described in the next section), Toray has joined arms with Waseda University with the aim of producing not only an RFID tag equipped with state-of-the-art ICs, but also an anti-collision scheme suitable for RFID multiple access in retail and logistics industries.

The rest of this chapter outlines the technical motivation of the joint research with Toray Industries, Inc. and the associated objectives which are based fundamentally upon developing a new anti-collision scheme for (passive) RFID systems.

3.3 Joint Research Objectives

The objective of this research is to develop an anti-collision scheme to enable multiple access RFID recognition designed for batch reading in the logistics and retail industries. Analysis, development and practical testing will be conducted throughout the research. Specifically, the objectives of the joint research (relevant to this thesis) are as follows:

a) Electromagnetic analysis of simplified multiple access scenarios of RFID systems with consideration of logistics and retail environments.
b) Consideration of ALOHA-based (time-domain) random access with incorporation of code domain multiplexing in an FPGA via VHDL.
c) Application specific integration of NOMA characteristics into the time domain ALOHA scheme to mitigate the shortcomings of random access.

3.4 Summary

The disadvantages associated with Silicon-based ICs has encouraged researchers world-wide to develop new innovations that are more low-cost and easier to manufacture without excessively compromising on performance. Using what is known as a roll-to-roll process, Toray Industries, Inc. has developed a world-first, low-cost, Carbon nanotube composite-based RFID tag IC semiconductor, with an unprecedented carrier mobility of $182cm^2V^{-1}$. The new Silicon alternative is capable of operating in the UHF bands, which further allows for increased RFID channel distances. The new composite semiconductor is a strong incremental step towards achieving smart logistics and retail environments in the future.

Chapter 4

Electromagnetic Analysis of Multiple Access Scenarios

4.1 Introduction

Smart logistics systems will be a driving force in achieving an intelligent society, streamlining future e-commerce and production-to-retail supply chains. A key enabling technology for these systems are multiple access Radio Frequency Identification (RFID) systems.

In particular, passive Ultra-High-Frequency (UHF) RFIDs are known to support greater throughput and channel distances as a function of their operating frequencies [11], suitable for large-scale smart logistics applications. Although multiple access schemes for such RFID systems have been studied to some extent by other institutional bodies, there have been less focus on the electromagnetic analysis of RFID systems that employ multiple access.

This chapter therefore presents an electromagnetic analysis of simplified multiple access scenarios that involve multiple RFID tags. The related work, analysis methods and results of this study are presented in this chapter, along with the implications for implementing multiple access RFID systems in FPGAs.

4.2 Related Work

The majority of related studies have focused on concurrent identification of RFID tags, via the development of multiple access schemes. Specifically, recent studies have aimed at the employment of NOMA [12], CDMA [13] and other novel schemes [14], [15], [16], [17] for RFID systems, in which their scope of study have been limited to achieving concurrent tag data acquisition. There have also been recent outputs studying the

electromagnetic changes in the bending of RFID tags [18], the dimensional sensitivity of inverted-F-type RFID antennas [19], as well as analyses concerning the near-field presence of materials around RFID tags [20], [21]. The investigations carried out in [18], [19], [20], [21] however, did not make considerations in their analyses towards the realization of RFID multiple access, i.e., only single tag scenarios were considered. The work in [22] considered a passive RFID system for retail environments. However, the analysis in [22] focused more on received power and signal coverage in a multipath channel. The authors of [23] presented a formulation of the coupling coefficient between two RFID antennas, in the absence of multiple access considerations.

This chapter, on the other hand, discusses the simulations in ANSYS High-Frequency Structure Simulator (HFSS) and experiments conducted to investigate and deliver the contributions as per the following:

- Development of a UHF RFID tag antenna for the purpose of analyzing scenarios applicable to RFID multiple access, in simulation.
- Analysis of field radiation and return loss resonance via simulation, followed by verification in experiment.
- Implications of observations with consideration of reader positioning in indoor environments.
- Comparison of the study with existing studies relating to the analysis of RFID tags for multiple access.
- Consequential implementation strategies for realizing a multiple access RFID channel via an FPGA (Field Programmable Gate Array) embedded system and its associated challenges.

4.3 RFID Tag Model

Antenna geometries for RFID tags typically fall under two design types - the meander line and inverted-F [24]. Both designs are based on a folding structure, which permits the miniaturization of the antenna whilst operating at the same design frequency. Despite the cost of efficiency and bandwidth as a result of the miniaturization, both designs have a widespread presence in the communications industry.

For the electromagnetic analysis, the meander line design was employed due to its simple periodic trace geometry, with reference to the studies in [24], [25], [26]. The meander line RFID tag (Fig. 5) designed for the purpose of electromagnetically studying tag-to-tag interactions consisted of 4 periodic meander- “turns” as detailed in [25]. The primary dimensions of the resulting tag are as shown in Table 1.

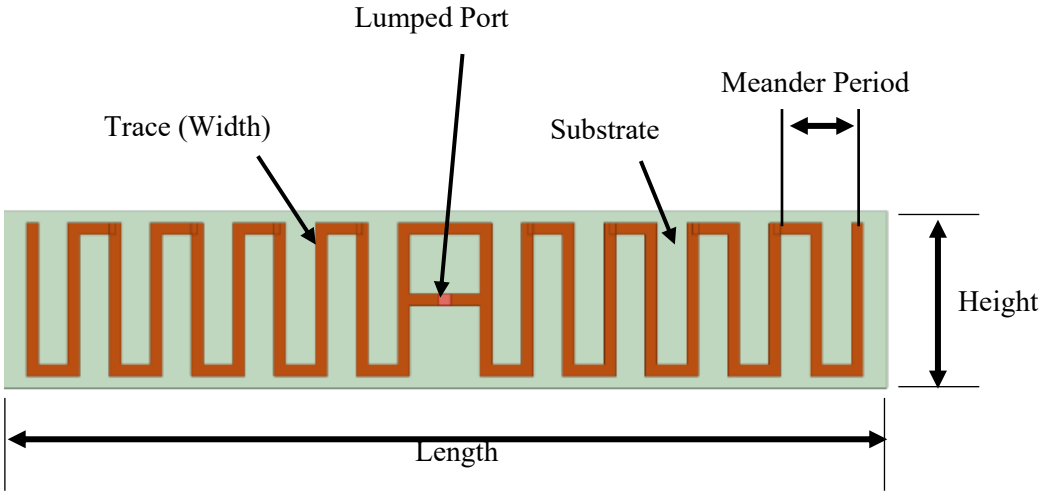

Figure 5. Meander line RFID tag used in simulation.

Parameter	Value
Length	75 mm
Height	15 mm
Trace Width	1 mm
Meander Periods (per side)	4

Table 1. Primary dimensions of simulated meander line RFID tag.

The full-wave solver ANSYS (HFSS) was used to visualize the scattering parameters and electromagnetics of the multiple access scenarios considered. The meander line underwent numerical optimization via the variation of the tag height to obtain a design operation frequency of 920MHz (UHF band).

4.4 Introduction to Coupling Scenarios

In logistics and retail environments, tagged items are likely to be arranged in an organized fashion, such as in Fig. 8. Intuitively, RFID tags on organized items will follow these arrangements. With this in mind, two 1D and one 3D arrangement scenarios were considered and analyzed in simulation. Fig. 6, 7 and 8 show the overlap, array and cubic scenarios considered respectively.

Case I: Overlap. Given that two or more tags are placed behind one another, the arrangement can be considered as an isolated overlap scenario, aligned along the y-axis (coordinate reference in Fig. 8). A tag spacing of $\lambda/8$ was used. A parametric analysis was performed by varying the percentage spatial overlap (1) of a mobile tag placed in front of a stationary (Fig. 6). The parameter α was varied along the x-axis (zero to 100 percent) of the tag length, $Ltag$, expressed simply as:

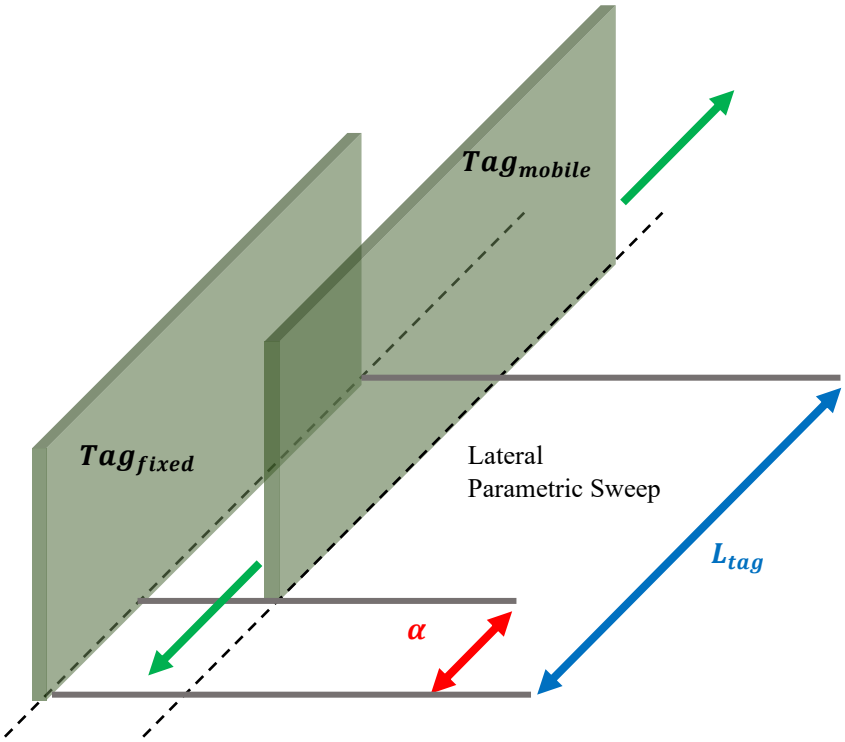

Figure 6. Diagram of Case I: Overlap.

$$Percentage\ Overlap = \frac{L_{tag}-\alpha}{L_{tag}} * 100\% \quad (1)$$

Case II: Array. If a user, for example, wished to read tags at the very front of a shelf, tags are considered to be in an array scenario. Tags would be arranged on a plane in parallel to the reader, i.e., on the XZ plane as in Fig. 8. For simplicity, the analysis of this scenario was considered only for tags along the z direction of the plane, and the array spacing was varied in steps of 10mm between 10mm and 100mm. A 3-tag model of this scenario is shown in Fig. 7.

Case III: Cubic. Case I and Case II considered 1D scenarios where their tags were situated along one direction (axis). To assess more real-world scenarios, arrangements in 3D were considered. Tags were placed in the x, y and z directions with respect to the tag at the cartesian origin as this better simulated a shelf or warehouse application. Fig. 8 shows the diagrammatic representation of this scenario. The cubic configuration was modeled using a reduced 27 (3x3x3) - tag arrangement to reduce computation time and memory overhead during simulation.

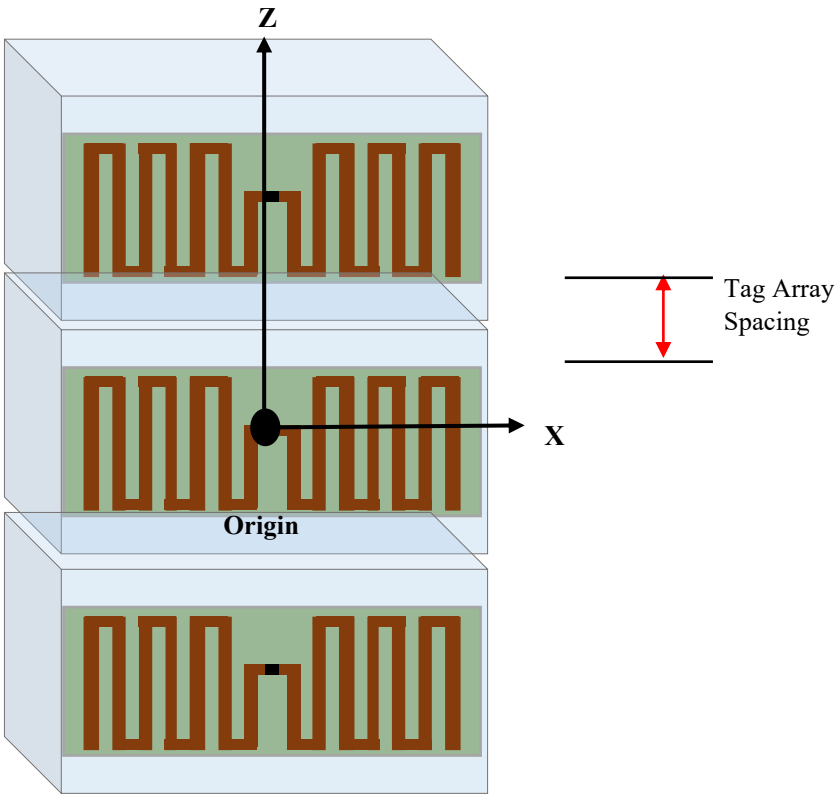

Figure 7. A 3-tag model of Case II: Array.

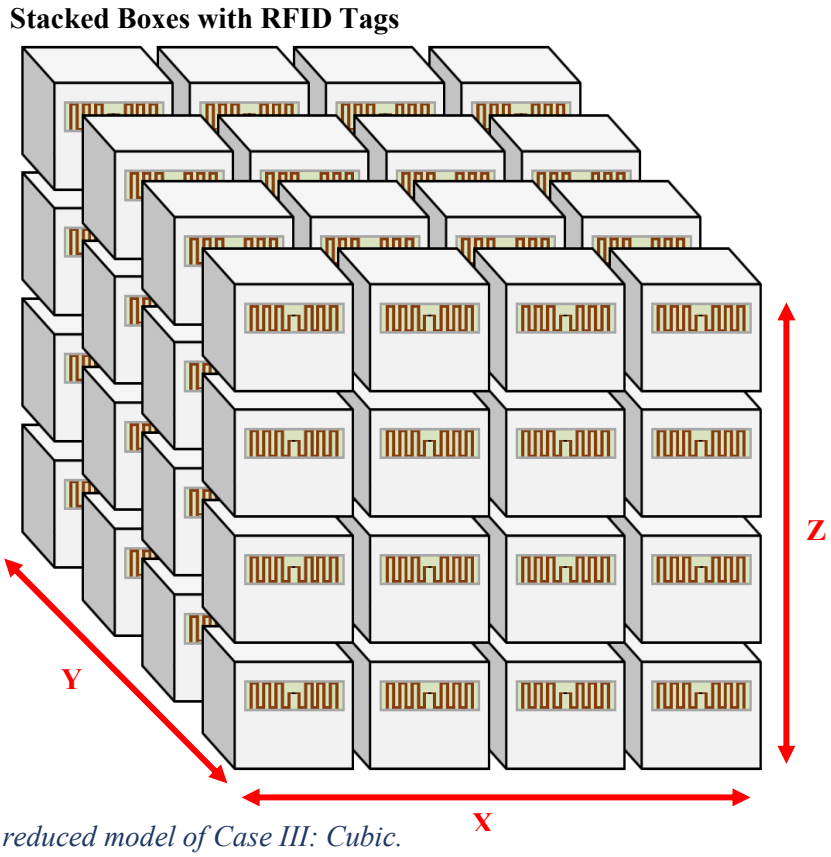

Figure 8. A reduced model of Case III: Cubic.

A separation distance of 200mm and 350mm was chosen for all x, y and z directions to simulate an organized group of cubic boxes, with the exclusion of box materials (e.g., cardboard) and internal contents (metal objects, lossy dielectrics) of the box. Knowing that the changes in far-field radiation will be less drastic with larger spacing, i.e., when tags are situated in the far-field region of every other tag, the separation distances were determined with reference to (2), (3) and (4). The successive separation distances were chosen to be smaller than 350mm to emphasize the sensitivity of field radiation with the presence of (parasitic) neighboring tags. The radiating field regions [27] were determined as per the following:

$$R_1 = 0.62\sqrt{\frac{D^3}{\lambda_0}} \tag{2}$$

$$R_2 = 2D^2/\lambda_0 \tag{3}$$

$$R_3 > R_2 \tag{4}$$

Where $R1$, $R2$, $R3$ are the reactive near-field, radiating near-field and far-field regions of antennas. The term D accounts for the largest dimension of the antenna, with a free-space operating wavelength of $\lambda 0$.

4.5 Comparison with Existing Studies

The primary difference between existing work such as those in [18], [19], [20], [21], [22], [23] is that the analyses presented in this chapter explicitly analyzes the electromagnetic characteristics for the purpose of understanding the challenges involved in realizing RFID multiple access systems. Specifically, the findings from this chapter will be used to determine the domain of the access scheme to be employed in future RFID multiple access development via FPGA system design.

The work in [18] studies the effect of bending of inverted-F type RFID antennas; [19] presents the influence of the mechanical dimensions of inverted-F type RFIDs on their resonance frequency – both of which only modeled one tag. The studies in [20] and [21] looked into environmental factors that affect tag identification performance, but again, only considered single-tag scenarios. The simulations conducted in [22] considered the effects of indoor retail environments on backscatter power via electromagnetic solvers and ray tracing methods. However, the analysis in [22] did not consider the implications of their findings on the realization of multiple access RFID systems. Similarly, although the authors of [23] presented a mathematical formulation of the coupling coefficient

between two RFID antennas, the work was constrained to near-field RFID systems without multiple access in mind. The analyses in this chapter were conducted with these differences in mind.

4.6 Simulation Results

Simulation of the scenarios were performed within an adaptive vacuum-filled boundary with a clearance from the outer most model objects of $\lambda/4$ (for 920MHz). Radiation boundaries were assigned to this region, and all conductive surfaces were assigned the perfect electrical conductor (PEC) boundary. A lumped port was situated at the center gap of each tag and excited with unity amplitude. The conductive traces were backed by a Polyethylene terephthalate (PET) substrate, with a thickness of 0.1mm and a corresponding relative permittivity, ϵr, of 2.25.

4.6.1 Overlap Configuration

Fig. 9 and 10 show the far-field radiation and return loss profiles for the overlap configuration respectively. By varying α (from (1)) between 0% and 100% of the tag length, notable distortions were observed in the far-field radiation.

From Fig. 9, it can be seen that at low overlap percentages of 0% and 25%, the upper azimuthal lobe is influenced by the directive characteristics of the mobile tag. With greater percentage overlaps of 75% and 100%, the mobile tag is alternatively seen to behave as a reflector, with the noticeable reduction in the upper lobe and increase in the lower.

The director and reflector characteristics suggest that the amount of overlap influences the electrical length of the mobile tag, with respect to the stationary. This behavior is comparable to Yagi-Uda antennas that exploit the directive and reflective characteristics of parasitic elements. However, for the use of RFID systems in multiple access, this characteristic is undesirable as it results in large, positionally-dependent variations in received power as well backscatter interference. It is important to note that this characteristic was more noticeable due to the short tag spacing, with which the mobile tag was situated in the reactive near-field region of the stationary tag.

Fig. 10 shows that the return loss resonance of the RFID tag was also observed to shift downwards in frequency with respect to percentage overlap. The total frequency shift totaled 30MHz, which can have considerable impacts on frequency division-based multiple access schemes.

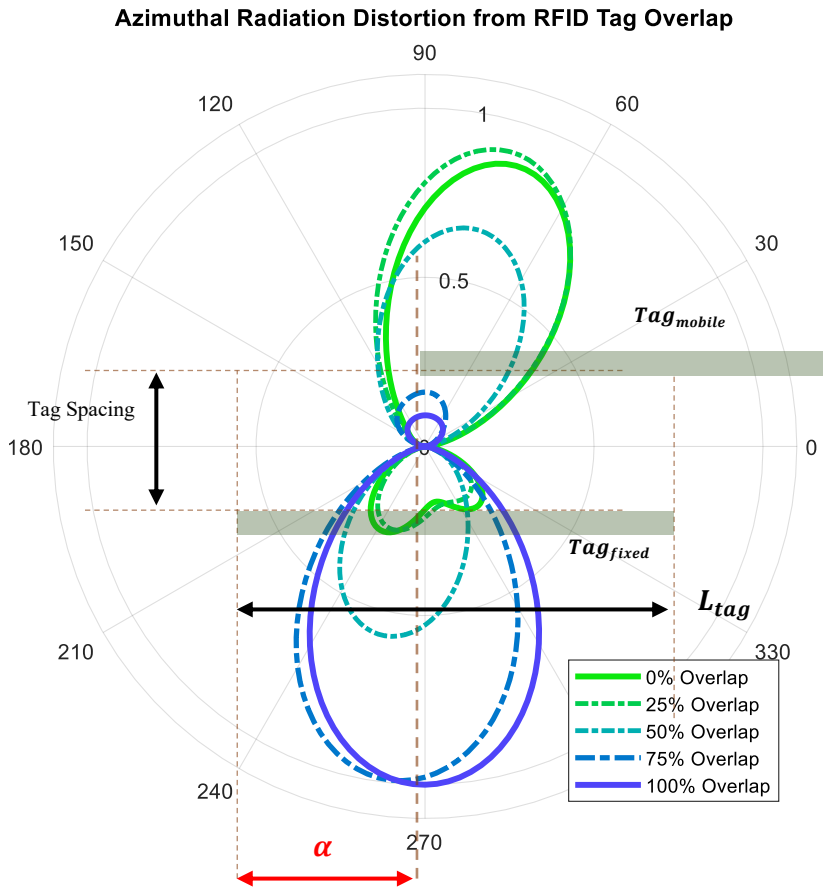

Figure 9. Far-field radiation (2D Polar) for Case I.

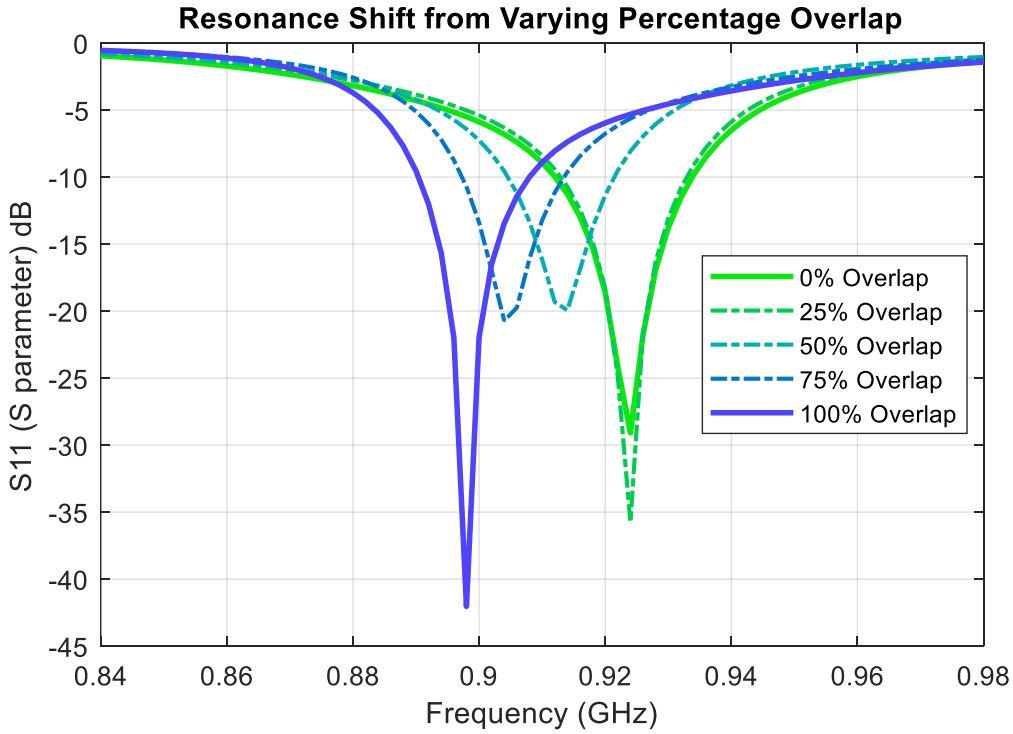

Figure 10. Return loss for Case I.

4.6.2 Array Configuration

The variation of array spacing across the chosen range (10mm to 100mm) resulted in noticeably large changes in field radiation, shown in Fig. 11. The smaller half (10mm and 30mm) of the simulated array spacing range resulted in fields radiating predominantly along the vertical array itself, i.e., the z-axis. This was similar to the directive effects observed in Case I. In the larger half of the parametric sweep (50mm to 100mm), fields are observed to be directed normal to the XZ plane of the array configuration, i.e., along the y-axis.

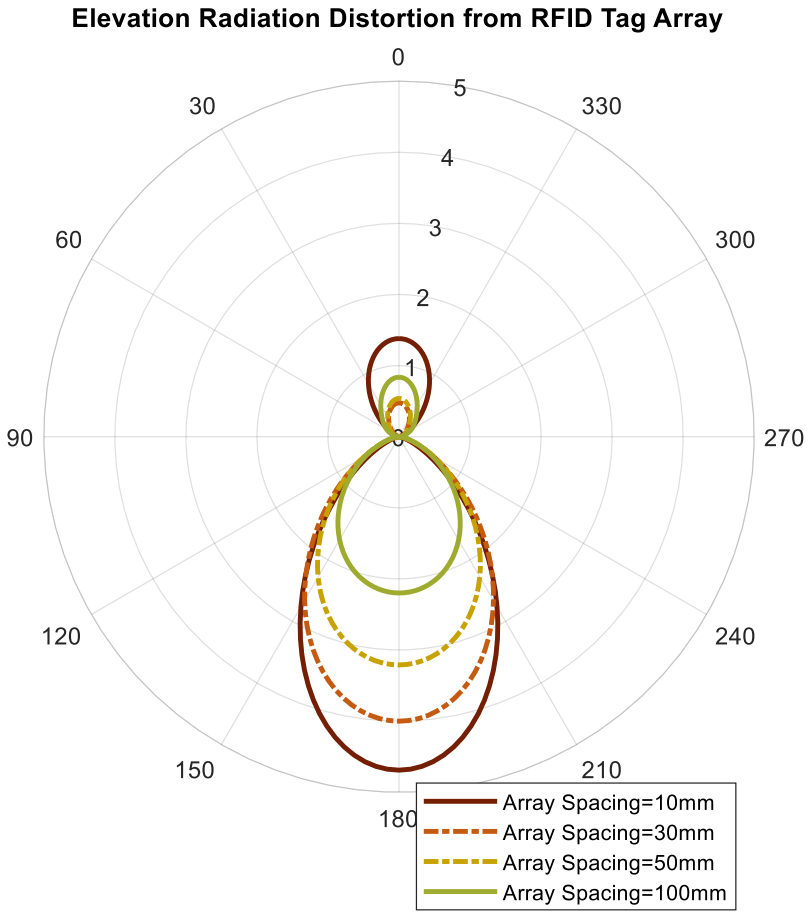

Figure 11. Far-field radiation (2D Polar) for Case II.

To better present the changes in field radiation, Fig. 12a and 12b show the 3D far-field radiation patterns for array spacings of 10mm and 100mm respectively. For an array spacing of 10mm, a narrow, negative z-directed lobe is observed along the plane of the array, whilst for an array spacing of 100mm, the main lobe is wider, and radiates relatively more power normal to the XZ plane.

Fig. 13 shows that there are notable reductions in the return loss resonance frequencies with the decrease in the array spacing. For an array spacing of 10mm, parasitic effects are observed via the emergence of an additional resonance spike. The shift in frequency shown in Fig. 13 is consistent with that in Fig. 10 for Case I, in that, the return loss resonance frequency of tags decreases with the decrease in tag-to-tag distances.

The similarity of Cases I and II simulations can be explained with the intuitive similarities of a meander line $\lambda/2$ dipole and a standard $\lambda/2$ dipole - both have the same donut shaped far-field pattern. Case I and II prove that despite the flat geometry of the meander line RFID tags, there are only minor electromagnetic variations arising from the lengthwise axial rotation of tags.

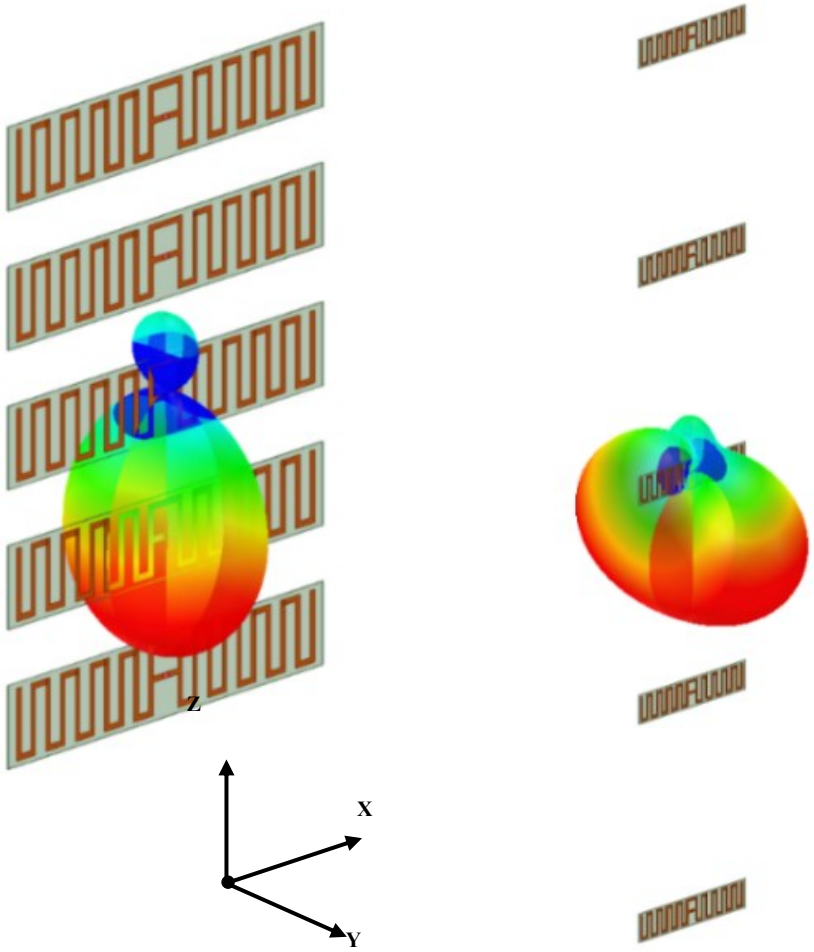

Figure 12. (a) 10mm spacing, (b) 100mm spacing. Far-field directivity (3D Polar) for Case II.

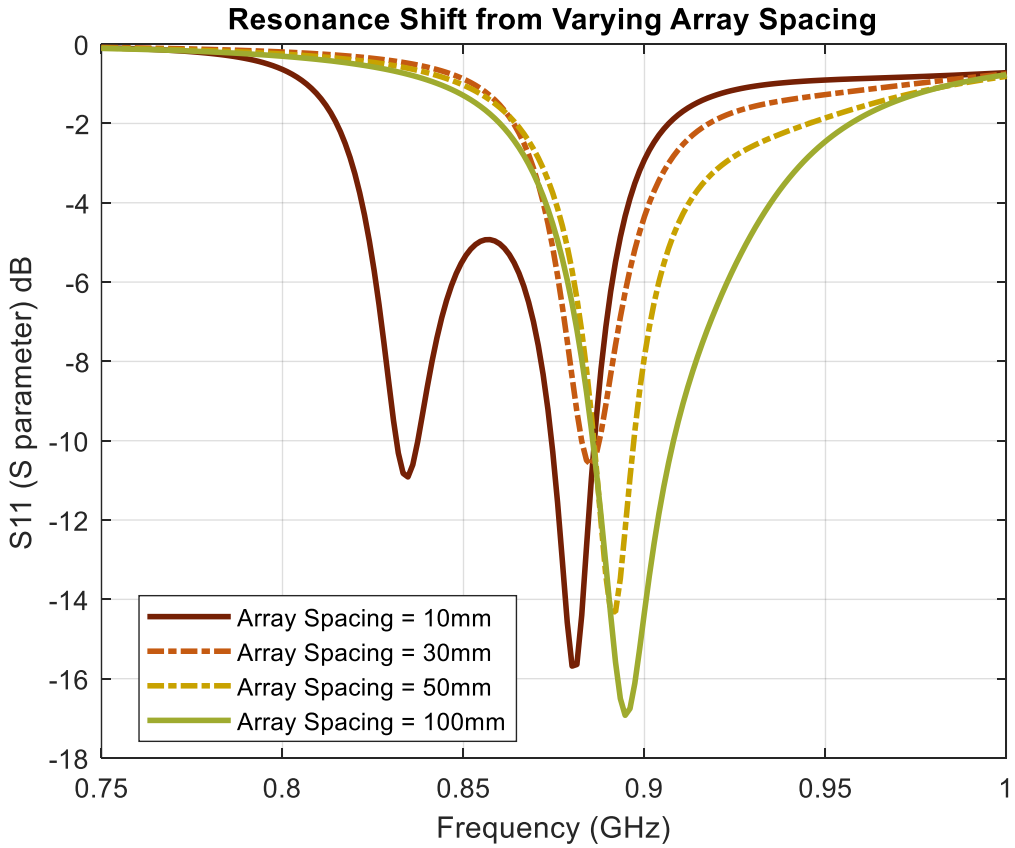

Figure 13. Return loss for Case II.

4.6.3 Cubic Configuration

The primary observation obtained from the cubic configuration was that when tags are arranged systematically in 3D space, it can clearly be seen that the resulting far-field radiation consists of lobes that largely correspond to each neighboring tag. Fig. 14 clearly shows this directive field behavior, where each significant lobe points in the direction of the tags surrounding the central tag.

With the reduction of the separation distance, the tags that were orthogonally adjacent to the tag at the origin began to behave as dominant parasitic elements and produced larger lobes (Fig. 15). A likely reason for this is due to the greater relative decrease in tag-to-tag spacing between the orthogonal tags and the one at the origin, compared to those positioned on the cubic diagonals.

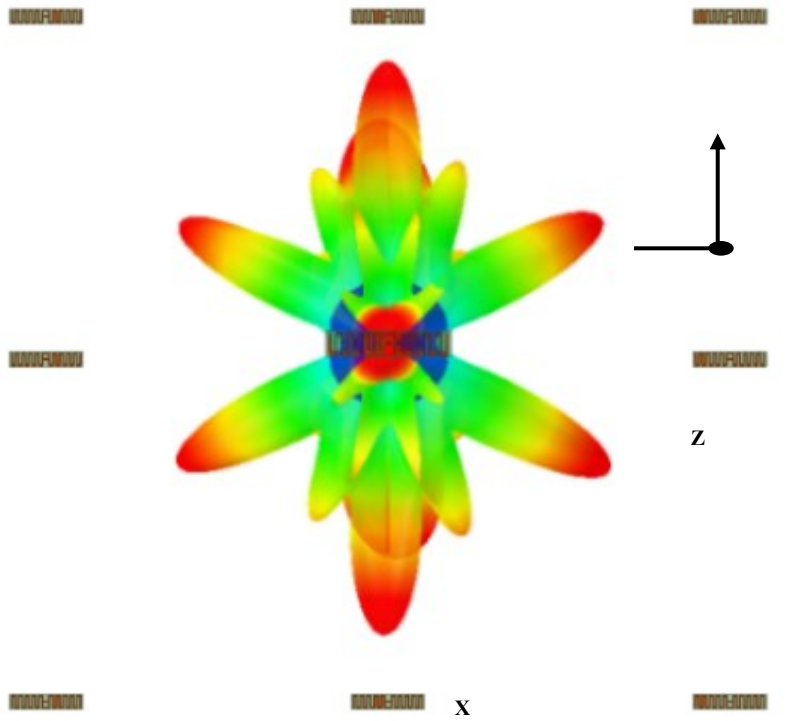

Figure 14. Far-field directivity (3D Polar) for Case III with 350mm separation.

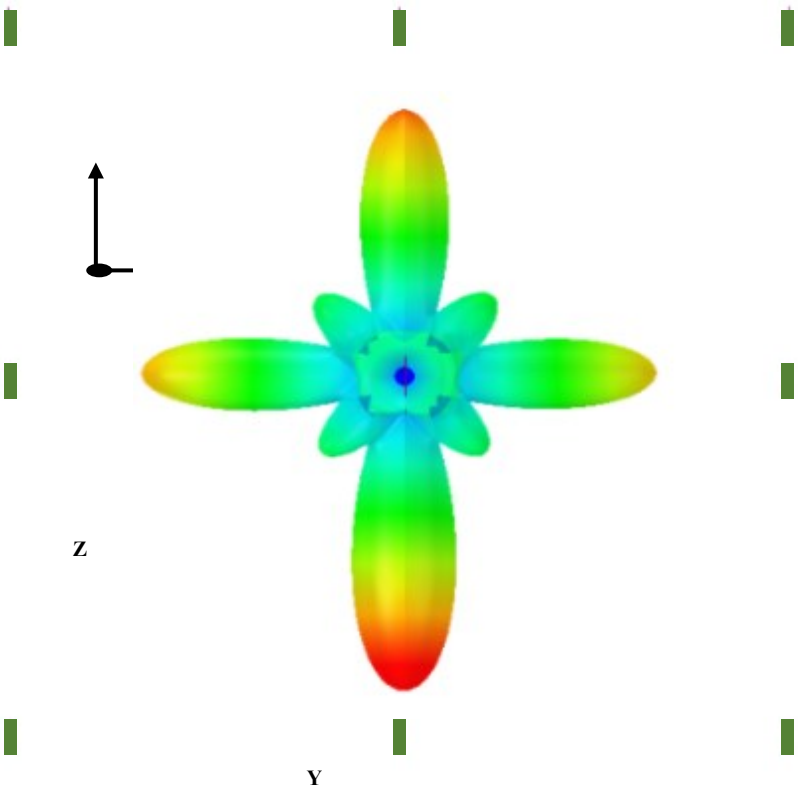

Figure 15. Far-field directivity (3D Polar) for Case III with 200mm separation.

4.7 Experimental Results

Experimental radiation pattern measurements were taken for the overlap scenario, i.e., Case I, to assess their agreement with the observations from simulation. Measurements were taken in an anechoic chamber with internal dimensions of 5.76m, 2.78m and 0.96m in length, width and height respectively. RFID tags operating at a frequency of 960MHz were used due to their immediate availability, and their Silicon semiconductors were removed to allow access to the trace terminals of each (total two) tag. Identical coaxial cables were soldered onto the tag terminals. The radiation pattern was measured via the received power of the overlapping tags, from a 960MHz transmitter dipole situated 3.5 meters away. The tag spacing was identical to that in simulation, of $\lambda/8$ and the transmission power from the dipole was set to -5dBm.

4.7.1 Measurement System

The measurement system consisted of a Keysight E5063A ENA Series Network Analyzer for transmission and reception, a desktop computer and a position controller for operating a stepper motor with a 2.5-degree angle step on which the overlapping tags were rotated. A diagrammatic representation and the realized system are shown in Fig. 16 and Fig. 17 respectively.

The overlap configuration was constructed using polystyrene as it is known to have a low loss tangent. The base and arm structures with which tags were suspended for varying degrees of overlap were all made of polystyrene.

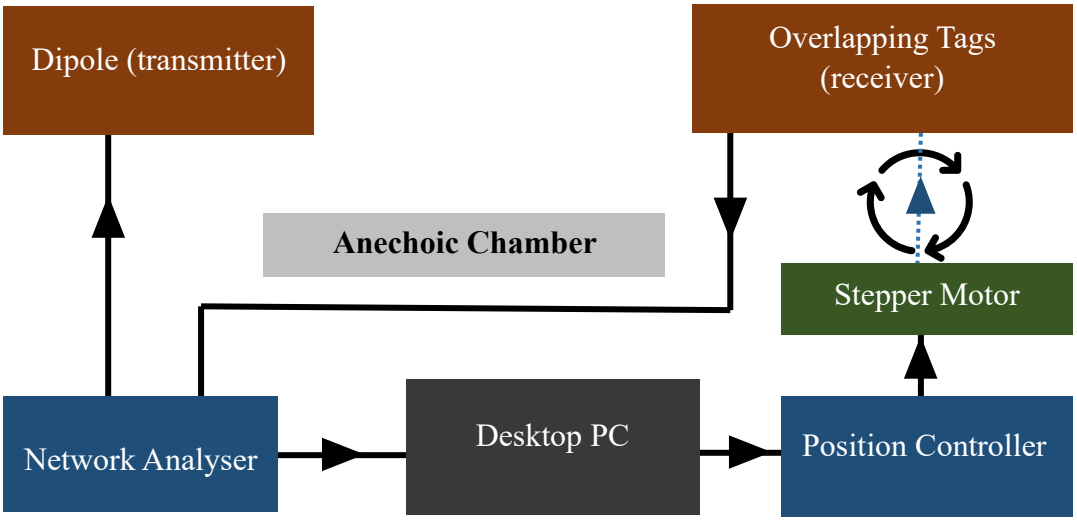

Figure 16. Diagrammatic representation of the practical measuring system.

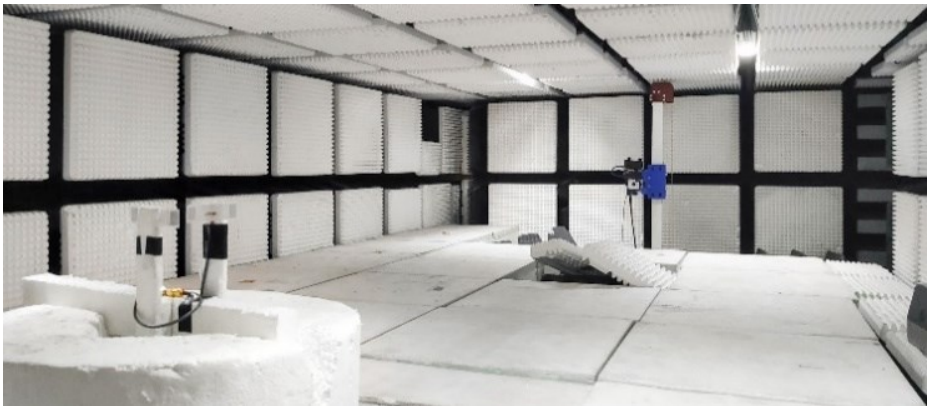

Figure 17. Realized system for radiation measurements.

4.7.2 Radiation Distortion for Case I

Fig. 6 shows the azimuthal radiation patterns measured via the experiment for the tag overlap scenario, i.e., Case I, as detailed in Section 4.4. The radiation pattern is in good agreement with that of the simulated, shown in Fig. 18, which practically verifies the director and reflector characteristics that occur in the presence of neighboring tags.

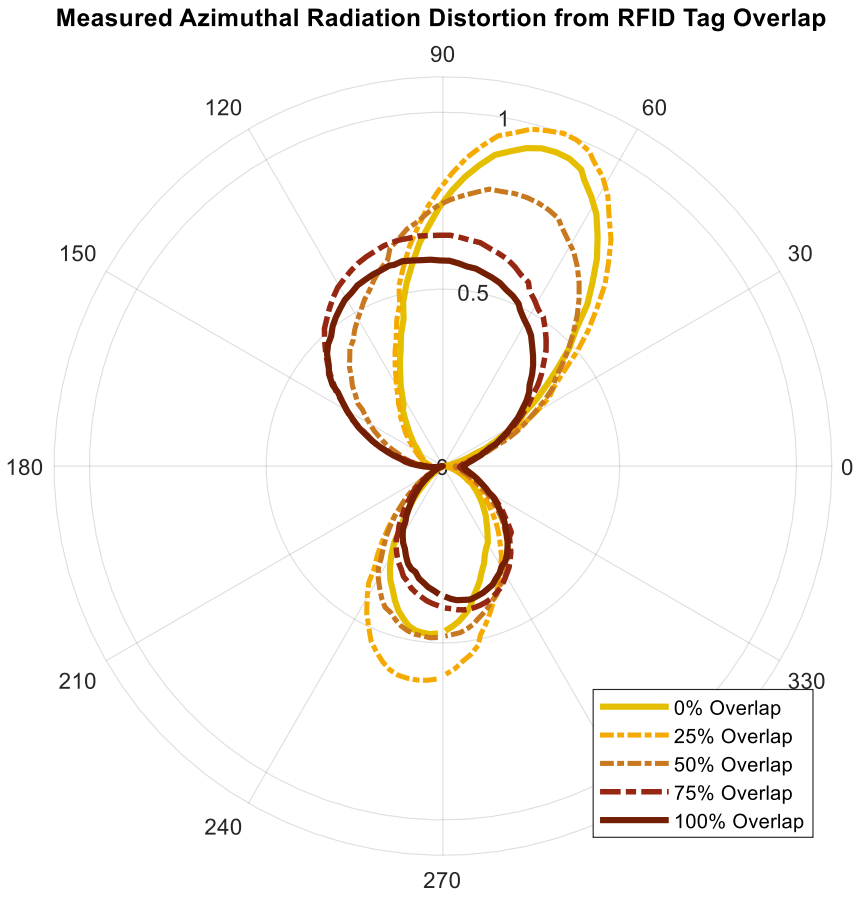

Figure 18. Measured far-field radiation (2D Polar) for Case I.

An important observation must also be made in that the measured radiation for 75% and 100% overlap appear to be rotated 180 degrees. A likely explanation for this rotated result is due to the rotational symmetry of the overlap scenario itself, i.e., there is no way of specifying the 'front' and' back' of the configuration electromagnetically.

4.7.3 An Important Consideration of the Results

In this chapter, both the far-field and spectral phenomena have been described and compared to that of Yagi-Uda arrays. The re-orientation of far-field directivity has been described via their relation to director and reflector characteristics. Similarly, spectral shifts have been justified based on the radiating regions of an antenna, viz: reactive near-field, radiating near-field and far-field.

Mutual coupling: However, the description of both the simulation and experimental results can be described more generally via what is referred to as mutual coupling. Mutual coupling (a term used in both communications and electronics) can be considered as electromagnetic interactions between two or more radiating devices to an extent where the behavior of one has an influence on the other, both in terms of radiation and frequency.

Impedance: Another important factor that has to be taken into account in the context of RFID systems is impedance. In most simulations, ports (where the energy is inserted into the problem space) are automatically assumed to have real, 50Ω or 75Ω impedance. Consequently, for a matched system, the device under simulations will also be designed to have the same, real impedance. For example, during the design of typical antenna geometries such as patch, bi-cone and monopole antennas the 50Ω match is desired and correct in simulation. However, in RFID systems, the load and source are complex (has both magnitude and phase) and are also thus a function of frequency. This is because tag ICs a mostly capacitive in nature due to their integration of many capacitive transistor elements.

Therefore, in simulating an RFID tag, there is, strictly speaking, a need to design the antenna that is matched in a complex impedance input port (where in which the port acts as both the complex load and source in place of an RFID tag IC). Furthermore, with the variation of frequency (as in a frequency sweep in simulation), there is ideally a need to make the port impedance frequency dependent in order to simulate varying impedance as a result of modulation for the reverse link.

4.8 Implications for RFID Multiple Access

Since realization is an essential step in developing and testing a suitable access scheme, the potential challenges in realizing a multiple access RFID system has been discussed in this section. The development of a multiple access scheme using an FPGA has also been considered with respect to the results obtained and has been discussed.

4.8.1 Challenges in Realization

Both simulation and experimental results suggest the need for multiple access RFID systems to support a degree of mobility in the tag readers as well as a form of intelligent control. Readers in a smart logistics application may require active repositioning using a predictive machine learning algorithm as a function of backscatter magnitude, relative to a standardized value.

Retail and commercial packaging will vary in size, which would influence whether tags will exist in the near or far field regions of their neighbors. In other words, attempts to acquire backscatter signals will also be hindered by what is effectively the 'steering' of lobes due to the constructive and destructive phase interactions arising from multipath backscatter signals, in addition to parasitic effects.

Furthermore, Fig. 10 and 13 show that frequency shifting resulting from changes in the relative spacing between tags were observed to be in the order of tens of megahertz. This magnitude of spectral variation becomes a non-negligible issue if the implementation of frequency-based multiple access schemes with narrow sub-carriers are considered for concurrent tag identification.

4.8.2 Influence on the Proceeding Embedded Systems Design

The simulations and experiments presented in this chapter visualizes the challenges associated with developing multiple access RFID systems. In the far-field, the variation of received power (at the reader) will be significant and thus, power domain methods which rely on successive interference cancellation (SIC) will be subject to high bit-error rates (BER). This is especially true for passive RFID tags which purely depend on harvested power.

Frequency domain schemes will be equally challenging to develop for RFID systems due to the tens of megahertz variation of tag operating frequency. In smart logistics, where tagged items will be stored in various arrangements it would be challenging to predict operating frequencies of tags. This would impede upon the realization of low-BER

frequency division multiple access. On this note, FPGA implementations of multiple access RFID systems in the near future will consequently be based on code domain frameworks, in which each tag will be assigned a pre-determined spreading code.

4.9 Summary

A simple meander line RFID tag has been developed to analyse scenarios that are applicable to multiple access RFID systems. The antenna was designed in HFSS an duplicated in simulation to analyse the electromagnetic interactions arising from the near-field presence of tags. The analysis was based upon the observations of far-field radiation and return loss. Of the three scenarios investigated, Case I was further analysed in the form of a practical experiments, with which good agreement with simulation was noted.

The results show that there are clear variations in far-field radiation depending on the degree of proximity of tags, whether they be arranged in an overlapped or array-like manner. The way in which the far-field varied has been compared to that of Yagi-Uda arrays, i.e., their director and reflector characteristics. Similar results were observed for the 3D case.

The analysis of the results confirmed that, for the future implementation of multiple access schemes via FPGA development, readers will require a considerable degree of sophistication to account for the mobility of tags (on items) and that, as suggested by the results, code-based access is preferred due to the wide spectral shifts that occur in tags when they are in close proximity to each other.

It was mentioned that, despite the results being compared to that of Yagi-Uda arrays, a more general term that encapsulates the observed behaviour is refer to as mutual coupling. An important consideration has also been noted, in that the impedance considered in both the simulation and experiments was real, and 50Ω. It was explained that this limits the representative accuracy of the work in this chapter because RFID tags operated fundamentally on complex impedance, that is, RFID tags have a complex load and source due to the highly capacitive impedance of tag ICs.

Chapter 5

FPGA-based Anti-Collision Conceptualization

5.1 Introduction

Field Programmable Gate Arrays (FPGA) are, as the name suggests, programmable instruments that can be configured to perform a plethora of functionalities. FPGAs contain many logics gates (transistors) that are software defined into sophisticated functional logics blocks and memory, as per the requirements of a wide range of embedded systems projects [28]. A major application for FPGAs is in the domain of wireless (and wired) telecommunications research.

In this chapter, a conceptual proposal of an anti-collision system based on a UART (Universal Asynchronous Receiver Transmitter) backbone and code domain multiplexing is presented with supplementary diagrams. CDMA was chosen via the finding from surveying as well as the findings made in the work presented in Chapter 4. Related work and a brief background on the relevant technology is followed by the proposed concept. Later in the chapter, initial simulations as well as the consideration of future implications for practical experiments are discussed and summarized.

5.2 Related work

There have been a number of studies related to multiple access implementation via FPGA development, within which a smaller number of published works focused on applications that are specific to the RFID domain.

Studies such as [29] focused on the performance evaluation of binary tree based anti-collision and investigated the speed with which the algorithm can identify a tag, as well as the efficiency of the algorithm. The work described in [30], [31], had more focus on code domain methods and provided a comparison with the time domain ALOHA method (which is currently the most common anti-collision method for RFID systems).

Hybrid schemes were also investigated in [32] where in which SDMA (Space Division Multiple Access) and TDMA (Time Domain Multiple Access) were combined. A multi-channel communication system based on UART along-side the FIFO (First In, First Out) method was implemented in [33].

5.3 Universal Asynchronous Receiver Transmitter

UART (Universal Asynchronous Receiver Transmitter) is a serial communications protocol used for wired links with a common baud rate of 9600 (bps), although this can be increased. UART can be configured to operate in half and full-duplex modes depending on system requirements, and this can be easily reconfigured in code. A typical UART transmission packet consists of a start bit, data bits and a start bit, with the option of adding parity bits. An example of an entire UART packet frame is shown in FIG 19.

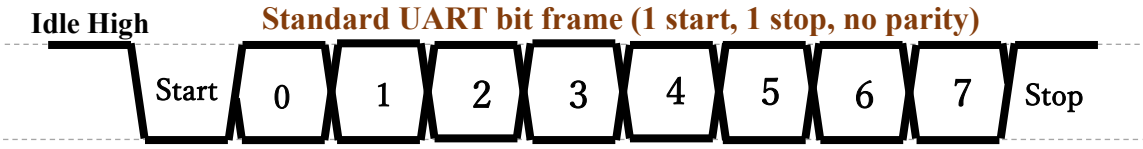

Figure 19. An example UART data packet structure.

5.4 CDMA Coding

CDMA, or Code Division Multiple Access is a multiplexing protocol with which orthogonal (zero or low correlation) codes are utilized to achieve larger signal capacity in a given channel for optimal channel resource utilization. CDMA is used in earlier cellular mobile networks such as second and third generation (2G and 3G) networks. Code division, however, was slowly driven out by newer schemes, such as OFDMA (Orthogonal Frequency Division Multiple Access) and NOMA (Non-Orthogonal Multiple Access).

CDMA spread sequence codes are typically generated as a pseudo-noise (PN) sequence. Such PN sequences are often generated using a software implemented Linear Feedback Shift Register (LFSR), which is practically a series of n-bit long flip-flops. This chain of flip-flops has feedback locations, known as taps, which determine the length of the pseudo-random sequence with a given n. The maximum possible sequence for a LFSR with length n is given by,

$$max.sequence.length = 2^n - 1. \quad (5)$$

As implied in (5), larger n results in longer sequences that can be considered practically random, but repeatable (pseudo-random) for experimental purposes. Intuitively, the taps should be located such that the sequency length is maximized for efficient use of the LFSR. For example, to enable maximum length sequences in a 16-bit LFSR, the tap (feedback) locations as noted in [34] are 16, 15, 13 and 4. Fig. 20 shows the resulting feedback loop with the XNOR (Exclusive-Nor) operations included.

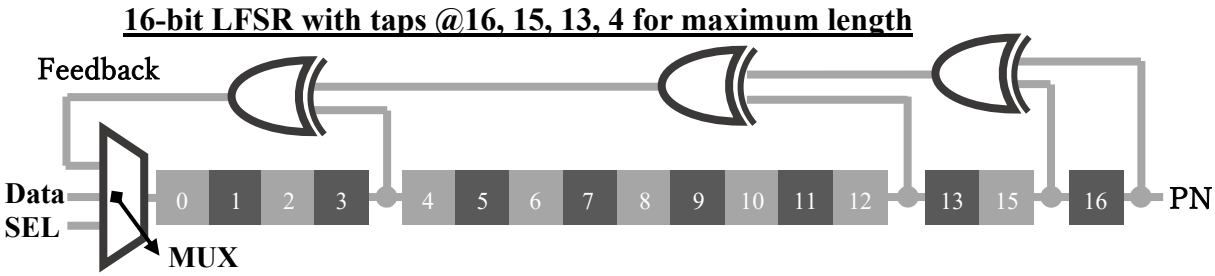

Figure 20. High level diagram of a 16-bit LFSR with taps.

5.5 Proposed Concept

For FPGA development, an embedded system is proposed in which the backbone transmission protocol of UART is utilized to form the basis of the communication system. CDMA coded and modulated (ASK, BPSK) streams can be pre-determined for each tag and stored as data in the tags. The advantage of this is that real-time digital signal processing (DSP) will not be required and will simplify transmission, despite the well-known fact that CDMA systems require relatively complex hardware configurations. Fig. 21 show a high-level visual of the system concept.

Expanding from the UART base program, the proposed concept will have an increased data bit frame from 8 bit to a very high number (i.e., will no longer be ASCII encoded serial UART). The increased bit count in the data frame will actually account for the chips of a CDMA spread spectrum (mostly) orthogonal code. The bits that actually represent data may still be 8 bits, but the transmitted bit stream will be of a higher resolution to account for the incorporation of the coding.

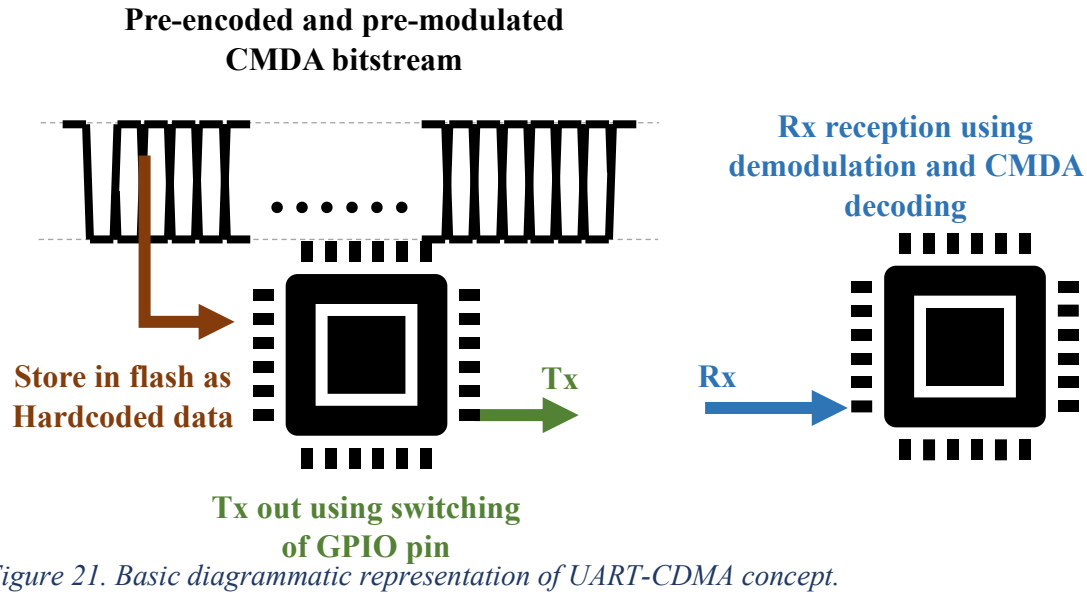

Figure 21. Basic diagrammatic representation of UART-CDMA concept.

5.6 Simulations

Simulations intended for FPGA development involve adding software-based clocks and custom error messages for debugging purposes. At the output, bitstream waveforms for each variable and signal defined in the software are shown. Such waveforms provide additional means of functional troubleshooting and verification prior to programming the FPGA.

5.6.1 Simulation Software

Xilinx offers two major versions of suites used for simulations, synthesis and programming. For 6th series and below (earlier), Xilinx ISE is used in a Linux virtual machine (if running on Windows machines). For 7th series and above, Xilinx provides another, newer package, called VIVADO, which can be run natively on Windows and other environments. Both suites offer largely the same functions, but which is smoother and more intuitively configured in VIVADO.

5.6.2 Testbench

It is good practice to test the software written in VHDL and Verilog prior to programming the target FPGA. For this purpose, it is common to build a software-based functional simulator often called a testbench within the development environment.

The entities defined in the source files are called into the testbench software as a component with which functions and the stimuli can be designed as per the test specifications. The simulated outputs found in this chapter were results obtained from operating the software-based entities using a testbench. This allows for detection of any logical errors within the architectures prior to practical testing on a physical board.

5.6.3 Initial outputs (UART Testing)

As mentioned in section XYZ, the proposed system is built off a UART backbone. Therefore, initial bitstream simulations (via Isim) were performed to confirm correct low-level byte transmission. For testing, a baud rate of 115200 was selected (this can be any standard rate) and a clock period of 100ns was used. Consequently, this resulted approximately 87 clocks per bit and thus a bit period of 8680ns.

With 8 data bits, 1 start bit and 1 stop bit per packet (10 total bits per packet) the packet period will be 86.8μs. To account for one packet transmission and reception each, the simulation time needed to be a minimum of twice that of the packet period, i.e., 173.6μs. Furthermore, to account for triggers and flags within the code, the value was rounded to

the nearest 100μs, i.e., the simulation time was set to 200μs. The resulting bitstream output (Isim) run in VIVADO suite is shown in Fig. 22.

Each row under the 'name' column represents either an internal signal, an input or an output (from the entity). The bright green bar (*test_Clk*) at the top is a visually condensed stimulus clock waveform with a frequency of 10MHz. With respect to this waveform the bit-wise transmission and flags are activated. For the transmission test, it is shown that for '*test_Tx_Serial_Bit_Out*,' the bits '*0110101011*' is transmitted. The first '0' represents the start bit (UART active low) and the last bit ('1') is the stop bit (idle high). In between the start and the stop bit are the data bits displayed backwards as the UART transmitter is designed to transmit the least significant bit (LSB) first. Upon the transmission of the stop bit ('1,' high), a transmit-complete flag is written high for one clock cycle and is shown on the row directly below the transmission serial stream. A similar observation can be made for the receiver entity, for which reception also occurs from the LSB. Since the UART is a serial communication protocol, the bits a received one at a time in a sequential fashion.

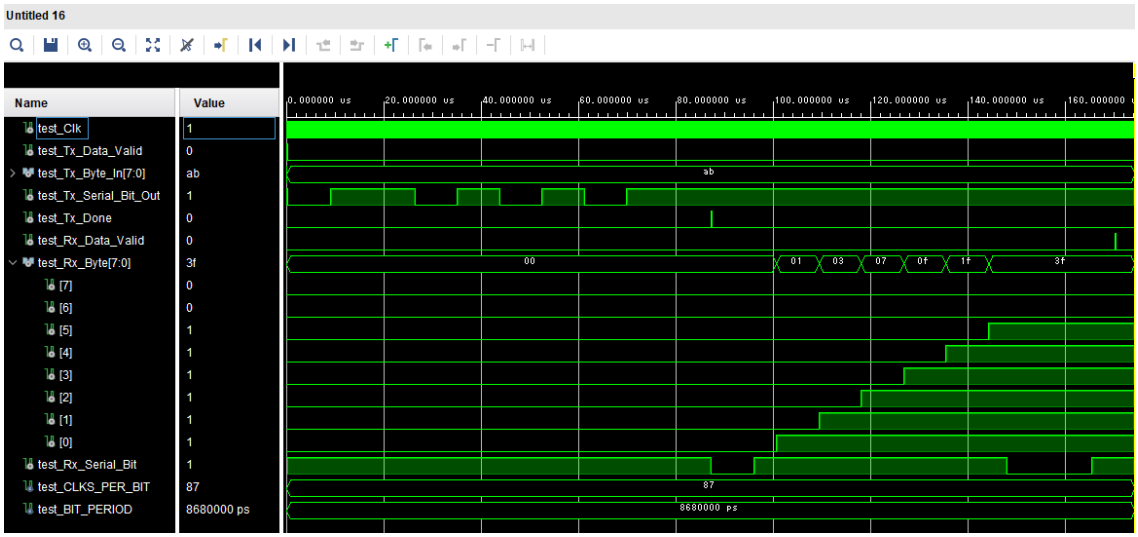

Figure 22. Bitstream output in VIVADO via Isim of UART base program.

5.7 Future Considerations and Challenges

Future simulations and experimentations of the proposed concept described in Section 5.5 will firstly involve the gradual incorporation of CDMA-like characteristics into transmission.

The experimental plan is to connect an FPGA to a signal generator (S.G.) and then to a tag antenna, or at least a representative radiating element, as shown in Fig. 23. The FPGA and S.G. will collectively act as the tag IC. Store data and pre-processed data are transferred (via a wired connection) to the signal generator, inside which the data is modulated to transmitted via the antenna.

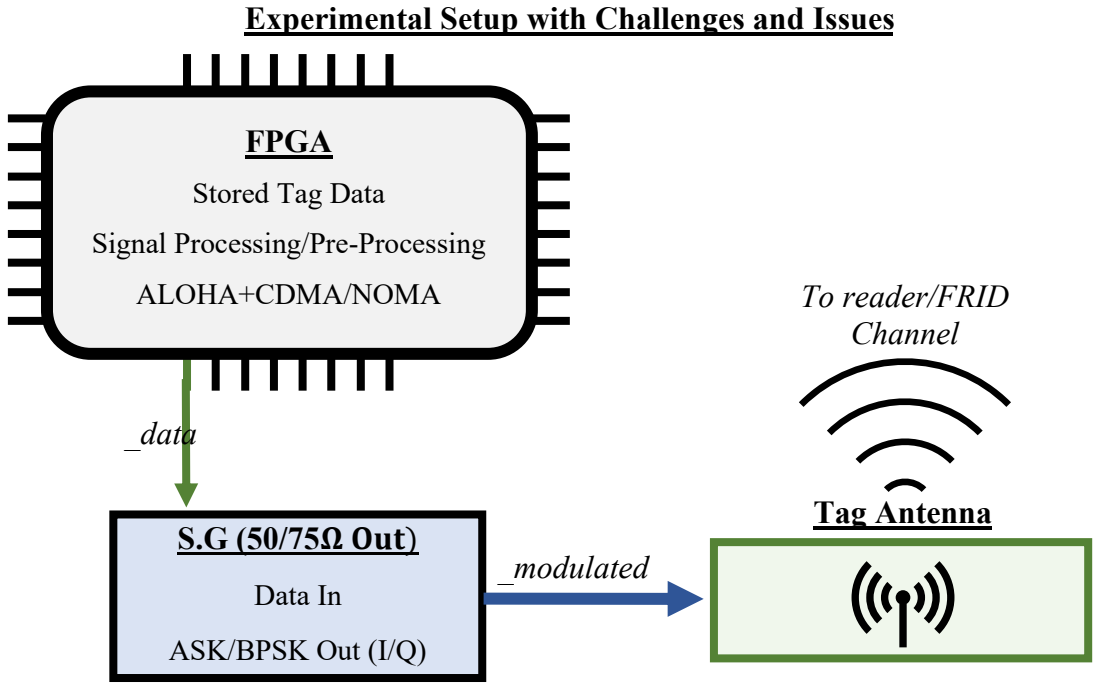

Figure 23. Diagram of future experimental with challenges.

The signal generator has variable power, and thus transmission power will be varied according to the needs of the experiment (but without over-powering the fragile antenna). However, this practical experimentation is expected to be accompanied by a number of challenges.

Impendence: A similar issue has been discussed earlier in Chapter 4 in Section 4.7.3. Typically, for an RFID tag, the tag IC acts as both the load (forward link) and also the source (reverse link) in the system. In addition, since the semiconductor switches used to construct logic gates and other circuitry inside the IC are made of capacitive thin-film transistors (TFT), the tag IC acts as a capacitive (complex) load and source. Therefore, during the different operating modes of an RFID tag, the complex impedance of the tag

changes as a function of frequency. This is an issue because, in FIG. 23, the use of a S.G. was described, which typically has 50Ω or 75Ω output impedance and are typically not variable beyond standard impedance values. This is not sufficiently representative of actual RFID systems because of the aforementioned impedance characteristics. Conducting experiments despite this issue may produce results that do not agree with simulations.

Energy Harvesting: A fundamental assumption made in the setup described in Fig. 23 is that the RFID tag harvested sufficient amount of power from the reader – an amount with which both the IC and the reverse link transmission can be powered. This means that in initially testing the system, a fundamental feature of passive RFID tags will not be considered. Although this may be a more acceptable assumption in comparison to the technical issue of impedance, the power requirements of the experimental system will likely be misjudged and will not represent an actual passive RFID system that harvests power. Energy harvesting is however, also challenging to reproduce in simulation, and thus, the assumption may have to hold in order to conduct experiments down the line.

RFID Reader: With the gradual development and experimentation of an anti-collision (multiple access) method for RFID systems, the only accurate way to practically test the systems is to also develop a reader. Naturally, the reader will have to have signal processing components that are specific to the transmission protocol that has been developed. This can create additional development time overhead and complexity.

5.8 Summary

An initial conceptualization of a CDMA and UART-based anti-collision method has been investigated with consideration of future FPGA implementation. The CDMA coding and all related pre-processing will be pre-computed and stored as data in the FPGA (which act as the RFID tag). VIVADO suite will be used to conduct bitstream simulations prior to practical testing. Although simulations could be conducted via idealized configurations, there are practical challenges that need to be addressed or sufficiently justified to bring an element of validity in the experiments. The challenges were discussed in the form of impedance, energy harvesting and the required implementation of a reader.

Chapter 6

An RFID System Assisted by the Internal Structure of Smart Refrigerators

(IEEE RFID 2022 Conference)

6.1 Background and Contributions

Despite the incredible benefits of incorporating SIC (Successive Interference Cancellation) into Slotted-ALOHA schemes [35], there is still a challenge in achieving sufficient power level differences (for SIC) upon packet collisions when the tags and scatterers randomly move in time [36] and are in short range – particularly for passive RFID systems.

In a refrigerator however, the contents inside will remain mostly stationary in time (with the exception of user access). A typical household refrigerator also consists of glass or polymer (dielectric) panels as shelves and separators to allow for organized internal real estate.

In this chapter, application specific advantages of household refrigerators are exploited and explored to offer the following contributions [37]:

- The proposal of an application-specific ALOHA-SIC anti-collision method for RFID systems in smart refrigerators.
- Analysis of power attenuation through the dielectric shelf panels with Ansys HFSS to achieve sufficient power level differences necessary for SIC.

6.2 Smart Refrigerators

As stated in [38], [39], smart refrigerators are one of many applicable outcomes that emerged from the concepts surrounding Internet of Things (IoT) where in which communication is established between machines (in addition to users) in response to ‘smart home’ aspirations. The term ‘smart’ is also associated by varying degrees of intelligence in the form of human-like decision making and automated alerts.

With added connectivity, there are also patented refrigerators with internet access for association with cloud-based platforms. The work in [39] provides an excellent high-

level overview of 'smart' functionalities that smart refrigerators could offer. Since a refrigerators primary purpose is food storage and medium to long term preservation, most of the functions revolve around internal content awareness, such as the recognition of content addition and removal, as well as other similar variants.

Detection and identification of internal contents may be achieved via user-assisted barcode or QR code scanning, or more recently, more autonomous RFID methods. In this chapter, focus has been placed on RFID-based smart refrigerators.

6.3 ALOHA-SIC Hybrid MAC

ALOHA-SIC is a hybrid multiple access scheme originally demonstrated by Choi [35], in which Successive Interference Cancellation (SIC) found in NOMA (Non-Orthogonal Multiple Access) - based schemes are incorporated into random access ALOHA to improve throughput without the need for additional spectral resources. As presented in Choi's work, given that there is an addition of a power level (i.e., number of power levels, L = 2) per orthogonal subchannel, B, theory proves that the throughput is 50 percent higher (1.5x) than that of ALOHA alone and can be derived from (6) with the appropriate substitutions.

$$Throughput_{ALOHA-NOMA}(L,B) = B\sum_{n=1}^{L} n\left(\prod_{m=1}^{n-1}\left(1-\frac{m}{L}\right)\right)\frac{e^{-\lambda}\lambda^{n}}{n!} \qquad (6)$$

It can also be shown (as also demonstrated by Choi), that if L = 1, that is, there is only one power level in each subchannel, the theoretical throughput is equivalent to that of ALOHA without power domain incorporation.

6.4 Related Work

Published work relating to RFID-based smart refrigerators have largely been software-oriented. Studies and proposed systems have focused on human interfacing of RFID systems and system prototypes that contain algorithms that offer 'smart' functionality. Specifically, related studies have proposed software-based systems that offer shopping reminders, recipe suggestions, and freshness detection [40], [41], [42] of food inside the refrigerator. Furthermore, there have been increasing interest in the incorporation of artificial intelligence into these software systems ahead of industry-wide aspirations for smart homes and cities. The difference to be noted here is that the aforementioned work focused on the software applications of an already working system, that is, the studies have assumed an already working RFID system inside a refrigerator. It is likely that such 'already working' systems operate purely off TDMA-based access.

Conversely, the work presented in this chapter concerns the development of an application specific anti-collision scheme for passive RFID systems, i.e., focuses on the anti-collision system between the tag and reader, in place of default time-domain methods used in current RFIC systems.

6.5 Proposed System and Concept Model

As heavily hinted in the preceding subsections of this chapter, the proposed system is composed of an application specific anti-collision method that is assisted by the internal structure of smart refrigerators. Specifically, given the knowledge of throughput improvements as a result of adding power domain features on top of time domain random access (Section 6.3 and [35]) the ALOHA-SIC scheme was chosen as the scheme of focus. Fig. 24 shows the diagrammatic frontal cross section of the proposed system.

The fundamental idea is that each time the interrogation signal passes through a dielectric shelf layer (in this case a glass panel), attenuation and horizontal energy scattering occurs. With each successive shelf, given that there is sufficient attenuation of some form, power levels can be established without the need for power control and allocation circuits within the tags themselves, thereby reducing tag manufacturing complexity and costs.

Since there is also an assumption that passive RFID tags are used, lower interrogation signal power harvested with each successive shelf, the available reverse link power will also be lower. The reverse link will also be subject to nearly identical attenuation paths as well, further contributing to the creation of power levels per shelf level. It is important to note that in the proposed model, the side walls are made non-conductive (unlike a typical refrigerator will a fully metallic enclosure) to allow for energy scattering out of the fridge.

In the case of the diagram in Fig. 24, there are two shelves which will create three power levels, given that the reader is situation at the top of the fridge internals. For the majority of packet transmissions, random access will be sufficient, and upon the occurrence of collisions, the power levels created via shelf attenuation will provide the necessary conditions for SIC. Fixed power allocation will be assumed for BER simulation.

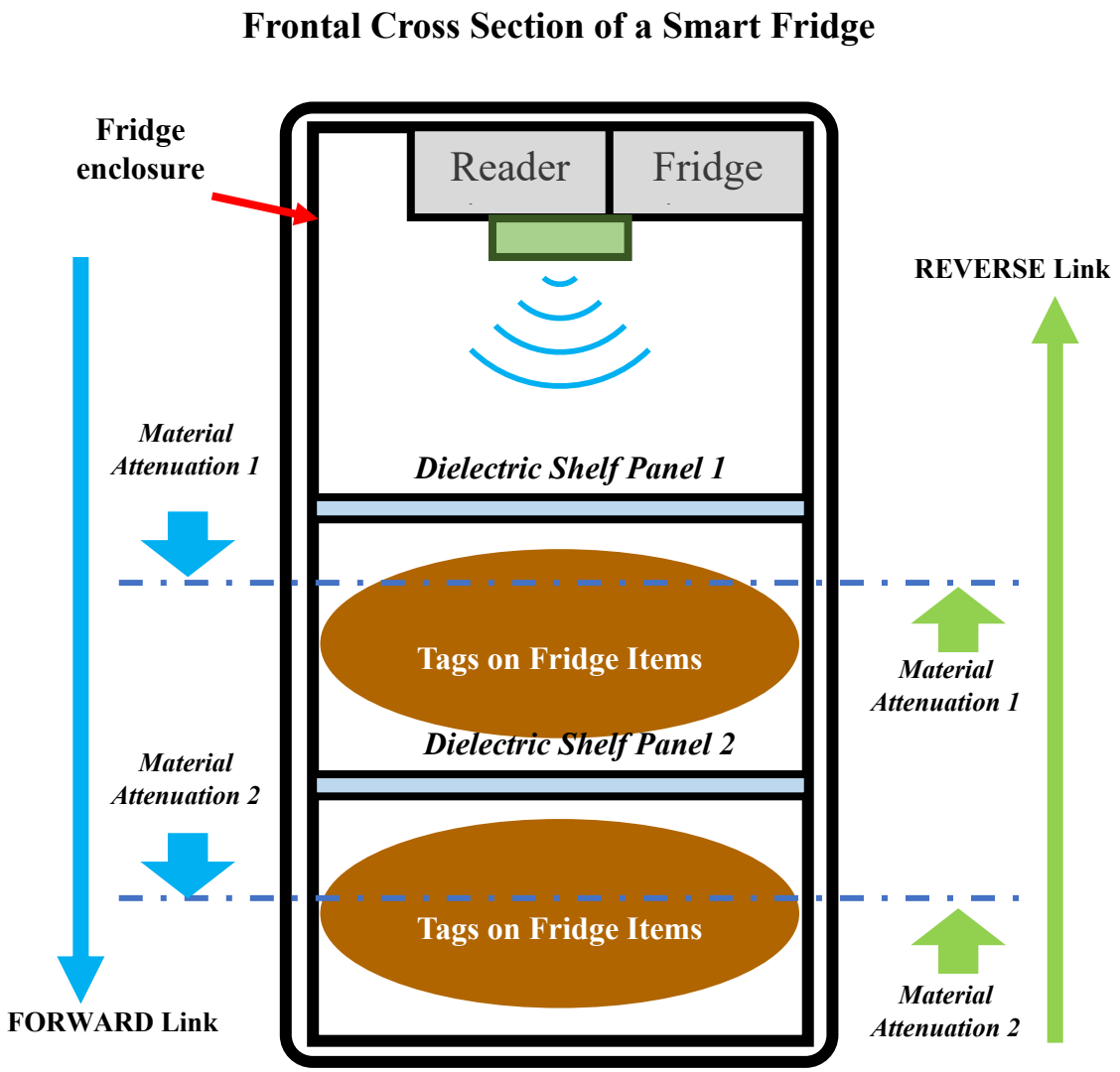

Figure 24. Diagram of proposed smart refrigerator anti-collision system.

6.6 Simulation Model

The refrigerator modelled in HFSS for analyzing the power levels created by the dielectric shelf panels is shown in Fig. 25 in dimetric view. A simplified representation of a refrigerator was created as it was deemed that minor details such as plastic compartments and door shelves would not contribute to large variations in simulation results, i.e., system performance.

RFID tags operating in the 860MHz -to 960MHz band (ISO/IEC 18000-6:2013) were placed halfway up each shelf. The reader antenna is situated 67mm below the top of the internal space. The internal space is enclosed (as in a closed fridge) by structural polystyrene with a thickness of 45mm. Note that as a bare minimum, a metal backing (required for fire safety [43]) and metal footing (for rigidity) are also added.

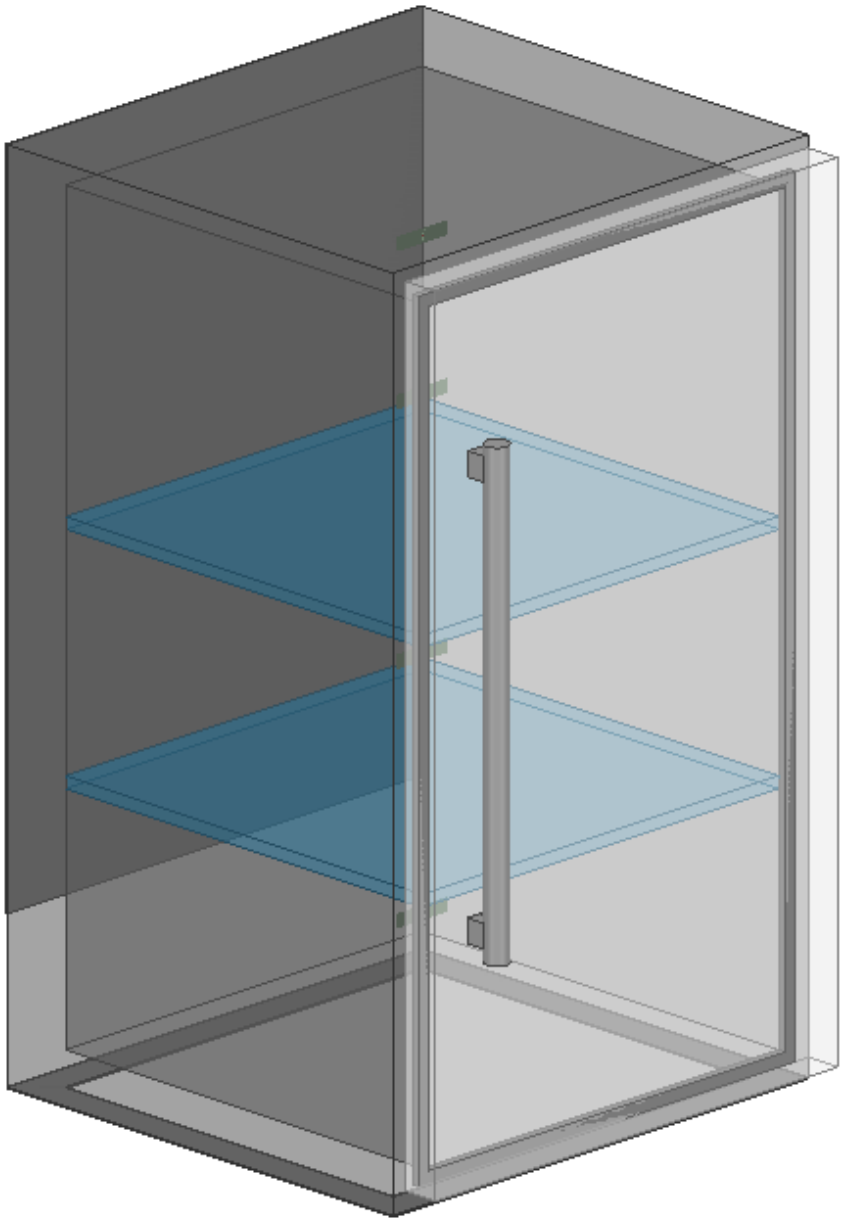

Figure 25. Dimetric view of a simplified refrigerator model.

Note that fridge contents were gradually incorporated into the simulations to allow for easier experimentation of the system concept.

The internal storage dimensions are 550mm in width and depth, and 1000mm in height. The refrigerator consists of two glass shelves (300mm apart) with a dielectric constant of 5.5. The remaining primary dimensions are shown as a third angle orthographic projection in Fig. 26.

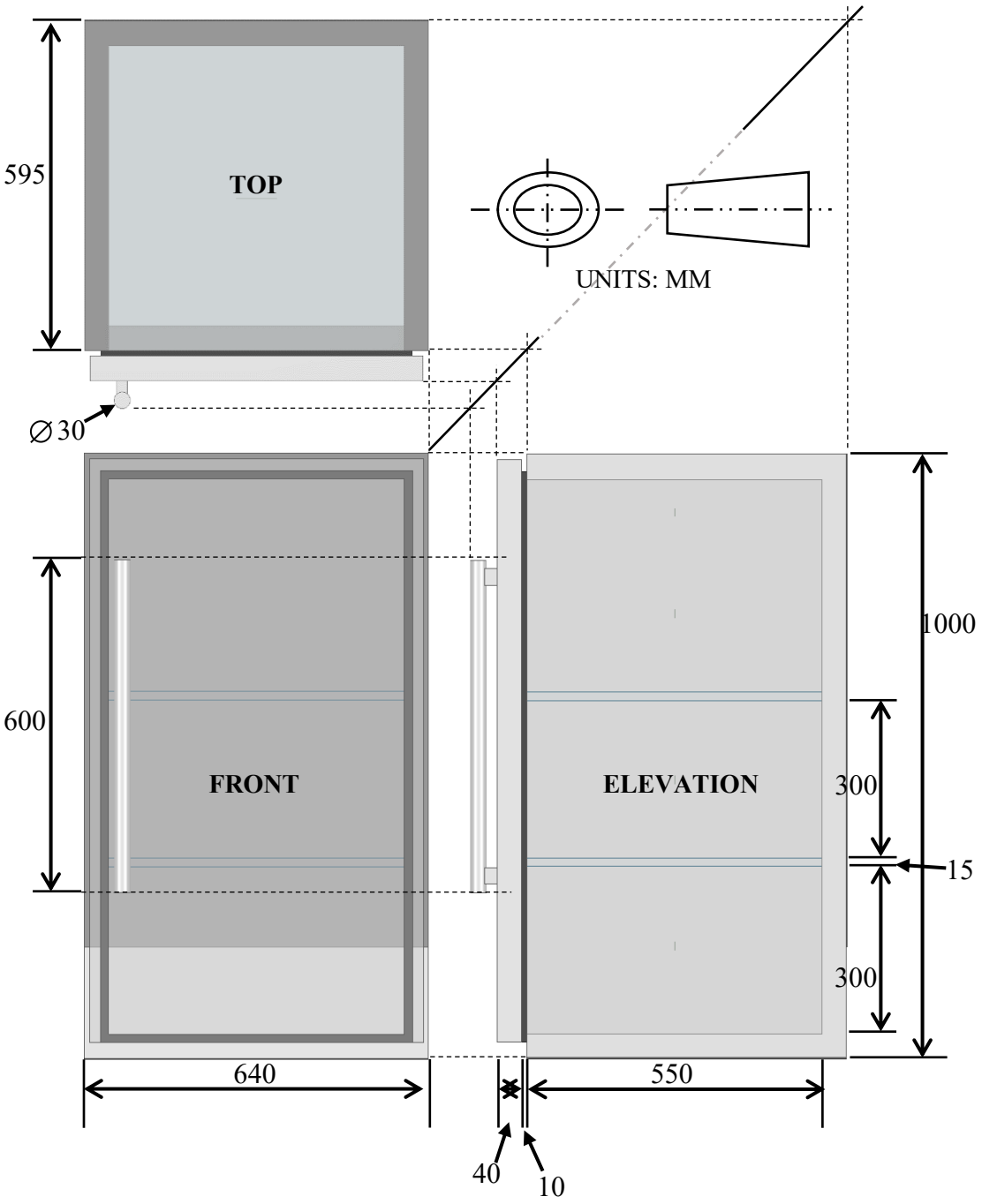

Figure 26. Third-angle orthographic projection of the refrigerator model.

6.7 Preliminary Simulation Results

Preliminary results in this chapter refer to results obtained in the early stages for the purpose of concept testing. In other words, preliminary results provide an additional incremental step towards concept system verification, prior to full system simulations as well as experiments down the project timeline.

Since the proposed system focuses on an application-specific concept, initial simulations were performed to verify whether the fundamental behaviors that were expected was reflected in the results. Specifically, observations were made as to whether the dielectric shelves provided any power attenuation (of any amount), and whether such attenuations from each power level (shelf level) created could be sufficiently differentiated from the cases where no (dielectric) shelves were placed inside the fridge. Results were obtained in the form of S-parameter S21 (insertion loss, with perfect match). Note that the same RFID tag design used for the study in Chapter 4 has also been used for the simulations in this chapter.

6.7.1 Empty Refrigerator Model

By obtaining the S21 value (in dB) from each reverse link and taking the difference with the S21 value from the successive power level (shelf) the relative received powers can be compared across the simulated frequency range. This gives a general idea as to how effective the dielectric panels are at producing power level differences between shelves. If the differences in S21 between two levels are greater with the presence of dielectric shelves, it would suggest that the shelves indeed contribute to the production of more distinct power levels. The comparison of S21 traces across the ISO/IEC 18000-6:2013 spectrum for the presence and absences of shelves are shown in Fig. 27, where the differences between the S21 magnitudes between each line signify the power differences.

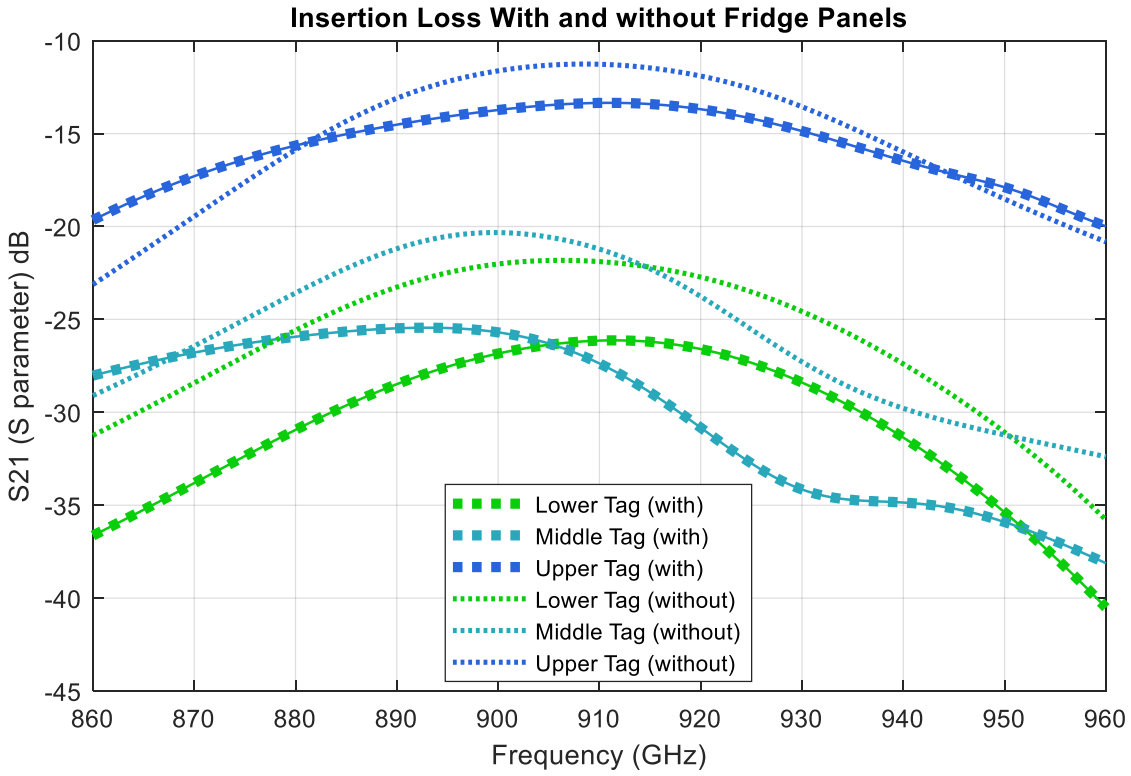

Figure 27. Insertion losses of the lower, middle and upper tags.

Results show that the power differences (between power levels) across the simulated frequency range were comparably greater with the presence of glass shelves, than the case without shelves. This suggested that each glass panel indeed contributed to additional attenuation and horizontal scattering of energy (enabled by non-conductive refrigerator side walls), resulting in less energy propagated in the direction of the reverse link. The preliminary result is encouraging and could lead to a higher success rate of SIC in the hybrid ALOHA-SIC scheme for RFIDs and consequently the improvement of BER.

6.7.2 Refrigerator Model with Simplified Water Bottles

The early indications from the first simulation that the dielectric shelves do in fact contribute to creating larger power differences brings promise to the proposed concept. However, real world refrigerators will almost always have content inside of them – all of which will have various electromagnetic properties.

For example, a water bottle would consist of not only the water (fresh, distilled, saline) but also the dielectric properties of PET (Polyethylene Terephthalate) that the bottle itself is made of. Meat and other liquids will also have temperature and state (e.g., raw or cooked, old or new) dependent permittivity.

To partially approach real world usage, water bottles with tags attached have been added to the simulation. Note that for simplicity, the water bottle structures (Fig. 28) are constructed purely of rectangular prism-shaped water, i.e., with the exclusion of PET or

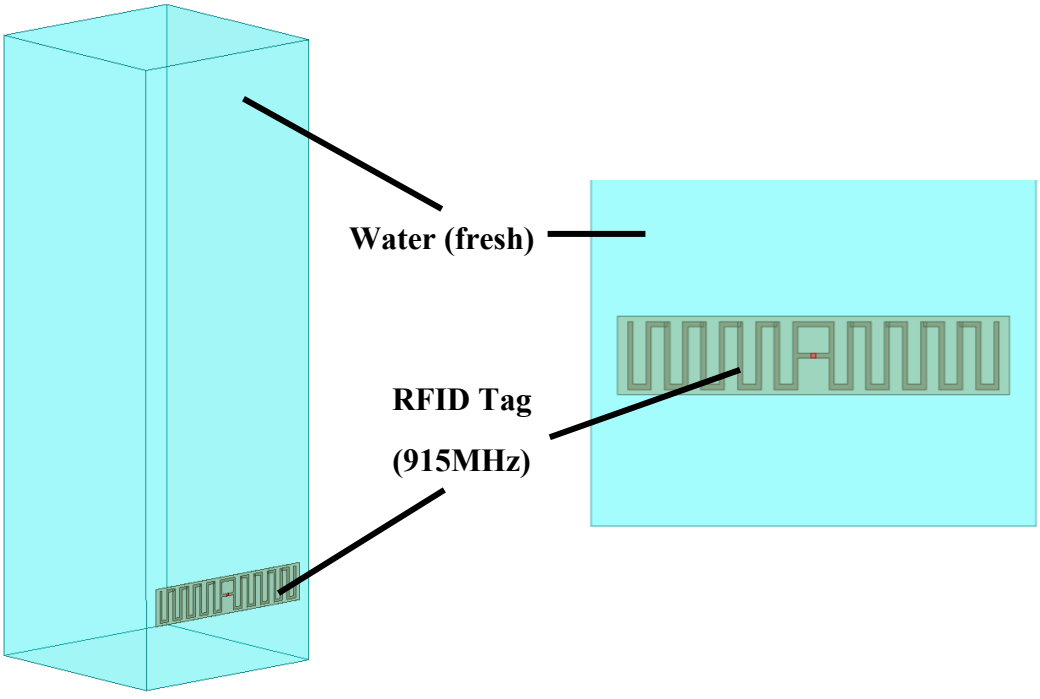

Figure 28. Simplified water bottle model for simulations.

any polymer-based bottle structures. The simulated bottle model has a height of 250mm with a width of 85mm in both horizontal directions. The RFID tag has been situated 25mm from the bottom of the bottle, as this could simulate the position of barcodes and other identification tools of the bottle, including an RFID tag. Note that fresh water has been used as the filler material.

The bottles (totaling 6) have been placed flush against the fridge door of the HFSS model, with the tags facing out (into the door) – three on the lower level and 3 on the upper level. The addition of six bottles (and therefore, tags) naturally results the addition of six additional excitation ports, along with the reader. A dimetric view of the model concerned is shown in Fig. 29.

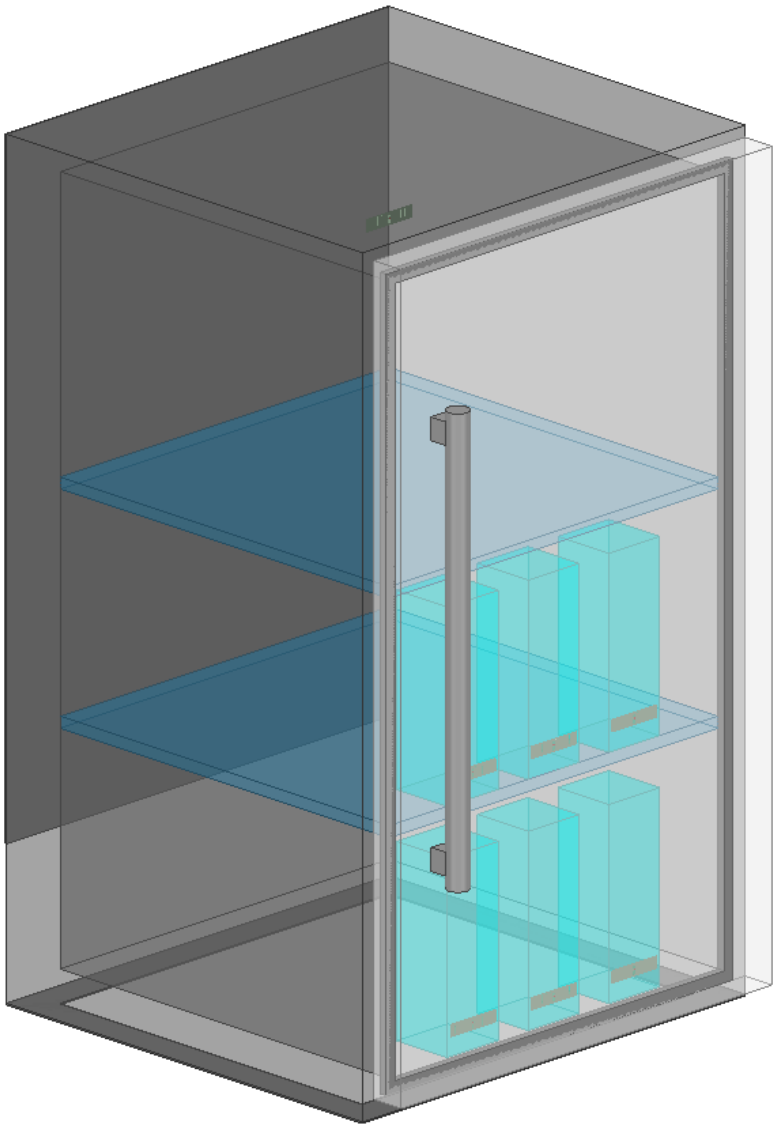

Figure 29. Dimetric view of the refrigerator model with water bottles.

The observations of the return loss (S11) begin to show the challenges that is associated with the further development of the proposed system. The S11 trace is shown in Fig. 30. All traces except for that of reader (in dotted red) show undesirable levels of energy reflection, with some spectral points approaching 0dB. This is likely due to the fact that the bottles were positioned flush against the door, with which large coupling effects with the dielectric doors changes the frequency characteristics of the tag (such as dielectric resonance). Another likely contributing factor is the highly conductive nature of water. The water bottle itself may be coupled with the tag, and in turn, acted as an inefficient antenna.

Since the passive RFID systems rely purely on harvested power, high return loss (i.e., close to zero) could considerably hinder the transmission quality (or even the ability altogether). Therefore, there is a need to explore the effects of complex impedance in simulation, if possible.

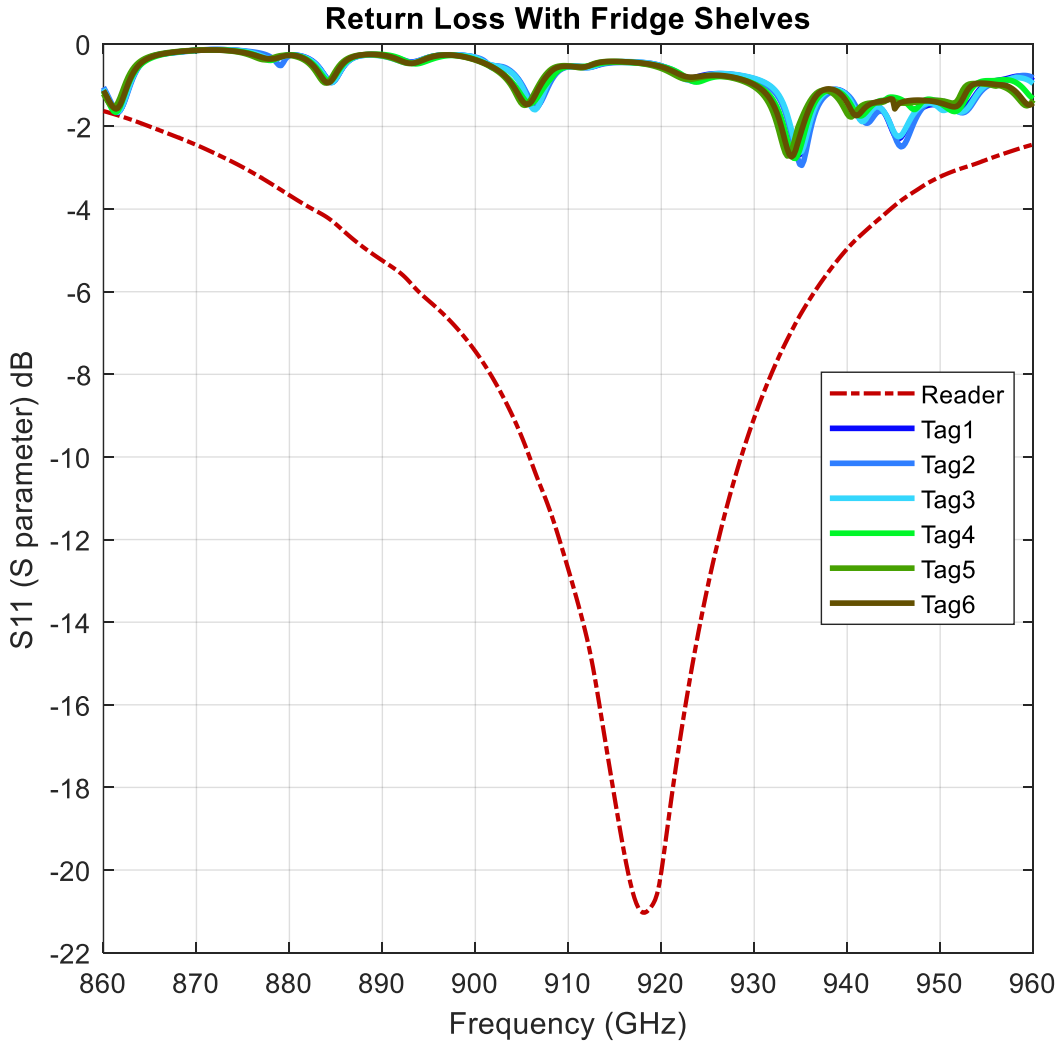

Figure 30. Return loss of ports in HFSS simulation of refrigerator.

6.8 Future Enhancements and Considerations

Since the ultimate objective of this concept is to develop an application specific anti-collision method for smart, RFID-based refrigerators, the simulations carried out in the future requires not only the consideration of electromagnetics, but also transmission quality. The investigation of the system in terms of BER (bit-error-rate) and transmission throughput is thus also necessary to verify the operation of the intended multiple access method.

Co-Simulation: This work will be extended by analyzing BER directly associated with the 3D electromagnetic simulation via a co-simulation between software, viz, Ansys HFSS and Ansys Electronics Desktop Circuit Simulator. The co-simulation will involve the port association between the nets of the circuit schematic and the excitation port in the 3D simulation. Output computations of transmission quality can be obtained via Ansys Electronics Desktop Circuit Simulator and the electromagnetic results from HFSS. This will allow for accurate use-case-specific simulations for BER analysis alongside field visualizations. The work from [35] will be used as reference to simulate the ALOHA-SIC.

Tag Positioning: To make future simulations (and potentially, experiments) as close to real-world scenarios as possible, various tag positioning and orientations need to be explored and investigated in terms of power level differences. Tag positioning can be further explored via the addition of more refrigerator content of difference material properties.

Complex Impedance Matching: Since the tags used in the simulations presented in this chapter were designed based on a 50Ω match with a 915MHz resonance, more work is required to explore complex impedance matching. In the presence of other refrigerator items, and in proximity to the refrigerator structures, the tag impedances will vary significantly. A potential method for investigation is the addition of inductive loops in the tag designs, or even in the refrigerator walls and shelves. Innovation in this area could result in more stable power level difference creation across the selected frequency range.

Simulation Time: Despite the necessity in simulations with more refrigerator content, the addition of more tags (items) naturally results in the addition of more excitation ports in simulation. Furthermore, a greater number of excitations in the presence of potential dielectric resonances and inter-item resonances will slow the convergence of the simulation. This means that the simulation will require a larger number of iterations and therefore more time, to maintain the same level of accuracy. A rough estimate of the

simulation time suggests that a moderately full refrigerator simulation may require simulation times in the order of tens of hours. This is because the simulation with the addition of simplified water bottles had a duration of 5.5 hours.

6.9 Summary

An application specific method for improving the hybrid ALOHA-SIC scheme was proposed. The idea is to exploit the propagation of energy through the dielectric shelves that already exist in a refrigerator, to create greater power level differences. The initial model was designed to have one door and two shelves. Results are promising in that the shelves offer larger insertion loss differences that in the case without them. The model with water bottles added to the simulation suffered from reflections and what is likely to be a large number of resonances. However, there were still signs of the effect of the shelves.

Research continuation requires the consideration of performing a co-simulation to obtain accurate BER results. Tag positioning, complex impedance should be further explored, whilst considering the impracticalities of extended simulation time, which could be in the order of tens of hours.

Chapter 7

Conclusions

In this thesis, focus has been placed on anti-collision schemes and applications relevant to passive RFID systems. Such systems are likely to make key contributions to smart logistics and cities in the future. Following the encouraging innovations (by a research entity) surrounding roll-to-roll-printed, carbon nanotube composite-based semiconductor RFID tag ICs, various research opportunities have emerged. The studies found in this thesis present various investigative pathways applicable to such state-of-the-art RFID systems.

Analyses, conceptualization and systems proposals have been communicated in their dedicated chapters, viz, 4, 5 and 6. The resulting observations were used to determine multiplexing domains that will be suitable for RFID systems, and to also bring insight into the expected challenges in future enhancement.

In chapter 4, (multiple access) RFID systems were highlighted as key enablers of future IoT and smart logistics networks. Challenges, however, still exist in this regime in that neighboring RFID tags (in close proximity) in a multiple access channel act as parasitic elements for one another. An RFID antenna operating at UHF 920MHz was developed for analyzing the electromagnetic behaviors of scenarios applicable to multiple access RFID systems. The results show severe changes in boresight angles depending on the percentage overlap of tags, which was verified by experiment. With small overlap, adjacent tags acted as directors and conversely as reflectors for large percentage overlap, implying that the percentage overlap changes the electrical length of the mobile tag, relative to the stationary. This was comparable to Yagi-Uda antennas. Return loss resonance was also observed to shift by 30MHz across the simulated overlap range, at a tag spacing of $\lambda/8$ m. Similar radiation and frequency characteristics were observed for the array configuration, likely due to the lengthwise axial symmetry of tags. In the 3D case, neighboring tags (with respect to the tag at the cartesian origin) were seen to direct the fields such that the 3D radiation patterns consisted of lobes corresponding to tag positions in the cartesian space. An important consideration was also made in that the analysis performed in this chapter were based off 50Ω matched antennas, with which the

results could differ from practical experiments with RFID tags operating with complex impedance. Regardless, the findings suggest that code domain may be the access scheme of choice, relevant to the implementation of multiple access RFID systems via FPGA system design in the near future.

The findings from Chapter 4 encouraged a conceptualization of a UART and CDMA based anti-collision method (over other multiplexing domains) for RFID systems, discussed in Chapter 5. The proposed concept is designed such that pre-processed CDMA signals are stored in the tags as data and modulated upon transmission. In this way, complicated signal processing circuits do not need to be designed for the tags. The system is planned to be implemented on a FGPA using a UART backbone. Through VIVADO suite, an initial simulation output has been produced to confirm the operation of the backbone UART program. It was concluded that there were several practical challenges that needed to be addressed for valid experiments. These practical challenges related to RFID impedance matching during experiments, consideration of energy harvesting (or lack thereof) during functional testing as well as the need for reader implementation at the experiment stage.

Chapter 6 considered an application of RFID systems in smart applications – namely, smart refrigerators. The proposed system exploits the (dielectric) shelves within refrigerators to provide additional power attenuation and in turn, produce greater power level differences. An initial simulation with a refrigerator model showed encouraging results in that, greater power level differences can be achieved with the presence of the shelves, that in the case without them. The model was extended with the addition of six simplified water bottles. However, it was observed that the radiation performance was hindered by what is likely dielectric resonance, as well as the coupling of tags with conductive water. It was determined that a co-simulation was required to observe more accurate simulation results that also include model specific BER analysis. Tag positioning and complex impendence matching will need to be further investigated. However, simulation time shall be kept in mind upon the addition of more fridge content in future simulations.

Academic Achievements

IEEE International Conference on RFID: Poster Session

G. Konishi, M. Saito, S. Shimamoto, S. Horii, S. Murase, “ALOHA-SIC-based RFID System Assisted by the Internal Structure of Smart Refrigerators”, in *16th IEEE International Conference on RFID (RFID 2022),* Poster Session, Las Vegas, NV, USA, 2022, (Accepted).

References

1) Denso Wave Incorporated, "*QR Code development story*," [Online]. Available: https://www.denso-wave.com/en/technology/vol1.html. [Accessed: 23-Jun-2022].
2) J. Costa, "*The History of the Barcode*," 2021, [Online]. Available: https://www.barcoding.com/blog/barcode-history. [Accessed: 23-Jun-2022].
3) S. K. Moore, "*How and When the Chip Shortage Will End*," 2014, [Online]. Available: https://spectrum.ieee.org/chip-shortage. [Accessed: 23-Jun-2022].
4) Toray, Ind. Inc., "*Toray Achieves World's First UHF Wireless Communication with Low-Cost Printed RFIDs that Could Be Retailing and Logistics Efficiency Game-Changers,*" 2020, [Online]. Available: https://cs2.toray.co.jp/news/toray/en/newsrrs02.nsf/0/F4FF9471A8CBCF16492584F5001F5352. [Accessed: 23-Jun-2022].
5) L. Silverman, "*Barcodes: A Brief History*," 2015, [Online]. Available: https://corp.trackabout.com/blog/barcodes-brief-history. [Accessed: 23-Jun-2022].
6) RFID Journal, "*What's the difference between passive and active tags?*,", [Online]. Available: https://www.rfidjournal.com/faq/whats-the-difference-between-passive-and-active-tags. [Accessed: 23-Jun-2022].
7) Advanced Controls & Distribution, "*Understanding RFID and RFID Operating Ranges*," 2017, [Online]. Available: https://blog.acdist.com/understanding-rfid-and-rfid-operating-ranges. [Accessed: 23-Jun-2022].
8) Toray, Ind. Inc., "*Toray Develops Semiconductor Circuits on Film by all Printing Process. Demonstrates wireless operations of RFIDs and sensors*," 2022, [Online]. Available: https://www.toray.com/global/news/details/20220114175355.html. [Accessed: 23-Jun-2022].
9) Toray Ind., Inc., Toray Logo, [Online]. Available: https://www.toray.com/global/. [Accessed: 23-Jun-2022].
10) A. Nikkaku, "*Message from the President,*" [Online]. Available: https://www.toray.com/global/aboutus/message.html. [Accessed: 23-Jun-2022].
11) R. Abdulghafor *et al*., "Recent Advances in Passive UHF-RFID Tag Antenna Design for Improved Read Range in Product Packaging Applications: A Comprehensive Review," in *IEEE Access*, vol. 9, pp. 63611-63635, 2021, doi: 10.1109/ACCESS.2021.3074339*).*
12) T. -H. Vu, T. -V. Nguyen and S. Kim, "Cooperative NOMA-Enabled SWIPT IoT

Networks with Imperfect SIC: Performance Analysis and Deep Learning Evaluation," in *IEEE Internet of Things Journal*, doi: 10.1109/JIOT.2021.3091208.

13) H. Shiomi, "Anti-Collision of RFID Tags with Blind DS-CDMA Using ICA," *2020 International Symposium on Antennas and Propagation (ISAP)*, 2021, pp. 47-48, doi: 10.23919/ISAP47053.2021.9391365.
14) K. Skyvalakis and A. Bletsas, "Asynchronous Reception of 2 RFID Tags," in *IEEE Transactions on Communications*, vol. 69, no. 8, pp. 5243-5254, Aug. 2021, doi: 10.1109/TCOMM.2021.3077942.
15) J. Mitsugi, Y. Kawakita and H. Ichikawa, "Concurrent backscatter streaming with batteryless sensors for wireless motion capture applications," *2021 IEEE 93rd Vehicular Technology Conference (VTC2021-Spring)*, 2021, pp. 1-5, doi: 10.1109/VTC2021-Spring51267.2021.9448926.
16) W. Sun, "Towards Parallel Decoding with Compressive Sensing in Multi-Reader Large-Scale RFID System," *2021 IEEE International Conference on RFID (RFID)*, 2021, pp. 1-8, doi: 10.1109/RFID52461.2021.9444387.
17) L. Han, J. Qi, X. Xie, C. He and Z. Jane Wang, "MPSK Orthogonal Coset Identification for Massive RFID Network," in *IEEE Communications Letters*, doi: 10.1109/LCOMM.2021.3108539.
18) A. S. Kashkool, A. I. Hammoodi and N. Alkhafaji, "Studying the Effect of Bending on Flexible Multiband Inverted-F Antenna for Wi-Fi/WiMAX Application," *2021 IEEE 19th International Symposium on Antenna Technology and Applied Electromagnetics (ANTEM)*, 2021, pp. 1-2, doi: 10.1109/ANTEM51107.2021.9518898.
19) Y. Fu, C. Huang, C. Gao and Y. Liang, "Study on inverted F-shaped RFID antenna," *2020 21st International Conference on Electronic Packaging Technology (ICEPT)*, 2020, pp. 1-4, doi: 10.1109/ICEPT50128.2020.9202948.
20) Y. Yu and Y. Qu, "Research on Environmental Factors Affecting RFID Reading Performance," *2020 IEEE 5th Information Technology and Mechatronics Engineering Conference (ITOEC)*, 2020, pp. 758-761, doi: 10.1109/ITOEC49072.2020.9141889.
21) F. Fuschini, C. Piersanti, L. Sydanheimo, L. Ukkonen and G. Falciasecca, "Electromagnetic Analyses of Near Field UHF RFID Systems," in *IEEE Transactions on Antennas and Propagation*, vol. 58, no. 5, pp. 1759-1770, May 2010, doi: 10.1109/TAP.2010.2044328.
22) Y. Chen and S. Chen, "Analysis of antenna coupling in near-field RFID systems,"

2009 IEEE Antennas and Propagation Society International Symposium, 2009, pp. 1-4, doi: 10.1109/APS.2009.5172382.

23) M. Škiljo, P. Šolić, Z. Blažević, and T. Perković, "Analysis of Passive RFID Applicability in a Retail Store: What Can We Expect?" *Sensors*, vol. 20, no. 7, p. 2038, Apr. 2020 [Online]. Available: http://dx.doi.org/10.3390/s20072038.

24) G. Marrocco, "The art of UHF RFID antenna design: impedance-matching and size-reduction techniques," in *IEEE Antennas and Propagation Magazine*, vol. 50, no. 1, pp. 66-79, Feb. 2008, doi: 10.1109/MAP.2008.4494504.

25) G. Marrocco, "Gain-optimized self-resonant meander line antennas for RFID applications," in *IEEE Antennas and Wireless Propagation Letters*, vol. 2, pp. 302-305, 2003, doi: 10.1109/LAWP.2003.822198

26) T. J. Warnagiris and T. J. Minardo, "Performance of a meandered line as an electrically small transmitting antenna," in *IEEE Transactions on Antennas and Propagation*, vol. 46, no. 12, pp. 1797-1801, Dec. 1998, doi: 10.1109/8.743815.

27) B. Constantine A., "Fundamental Parameters and Fig.s-of-Merit of Antennas," in *Antenna Theory: Analysis and Design*, 4th Ed. Hoboken, New Jersey, USA: Wiley, 2016, ch. 2, pp. 32

28) E. Monmasson and M. N. Cirstea, "FPGA Design Methodology for Industrial Control Systems—A Review," in *IEEE Transactions on Industrial Electronics*, vol. 54, no. 4, pp. 1824-1842, Aug. 2007, doi: 10.1109/TIE.2007.898281.

29) H. Ning, Y. Cong, Z. -Q. Xu, T. Hong, J. -C. Zhao and Y. Zhang, "Performance Evaluation of RFID Anti-Collision Algorithm with FPGA Implementation," *21st International Conference on Advanced Information Networking and Applications Workshops (AINAW'07)*, 2007, pp. 153-158, doi: 10.1109/AINAW.2007.286.

30) X. Hui and E. C. Kan, "Collaborative Reader Code Division Multiple Access in the Harmonic RFID System," in *IEEE Journal of Radio Frequency Identification*, vol. 2, no. 2, pp. 86-92, June 2018, doi: 10.1109/JRFID.2018.2852484.

31) G. Mazurek, "Active RFID System with Spread-Spectrum Transmission," in *IEEE Transactions on Automation Science and Engineering*, vol. 6, no. 1, pp. 25-32, Jan. 2009, doi: 10.1109/TASE.2008.917091.

32) H. Saadi, R. Touhami and M. C. E. Yagoub, "Design and simulation of anti-collision RFID system based on SDMA-OFDM," *2014 International Conference on Multimedia Computing and Systems (ICMCS)*, 2014, pp. 1510-1515, doi: 10.1109/ICMCS.2014.6911254.

33) S. Yu, L. Yi, W. Chen and Z. Wen, "Implementation of a Multi-channel UART Controller Based on FIFO Technique and FPGA," *2007 2nd IEEE Conference on*

Industrial Electronics and Applications, 2007, pp. 2633-2638, doi: 10.1109/ICIEA.2007.4318890.

34) P. Alfke, “Efficient Shift Registers, LFSR Counters, and Long Pseudo-Random Sequence Generators,” Xilinx XAPP052, 1996, [Online]. Available: http://ebook.pldworld.com/_Semiconductors/Xilinx/DataSource%20CD-ROM/Rev.4%20(Q2-2001)/appnotes/xapp052.pdf [Accessed: 23-Jun-2022].

35) J. Choi, "NOMA-Based Random Access with Multichannel ALOHA," in *IEEE Journal on Selected Areas in Communications*, vol. 35, no. 12, pp. 2736-2743, Dec. 2017, doi: 10.1109/JSAC.2017.2766778.

36) Hanshen Gu and Dong Wang, "A Content-aware Fridge based on RFID in smart home for home-healthcare," *2009 11th International Conference on Advanced Communication Technology*, 2009, pp. 987-990.

37) G. Konishi, M. Saito, S. Shimamoto, S. Horii, S. Murase, “*ALOHA-SIC-based RFID System Assisted by the Internal Structure of Smart Refrigerators,*”, IEEE RFID (Poster Session), May 2022. (Accepted, unpublished).

38) H. -H. Wu and Y. -T. Chuang, "Low-Cost Smart Refrigerator," *2017 IEEE International Conference on Edge Computing (EDGE)*, 2017, pp. 228-231, doi: 10.1109/IEEE.EDGE.2017.41.

39) A. Floarea and V. Sgârciu, "Smart refrigerator: A next generation refrigerator connected to the IoT," *2016 8th International Conference on Electronics, Computers and Artificial Intelligence (ECAI)*, 2016, pp. 1-6, doi: 10.1109/ECAI.2016.7861170.

40) L. Xie, Y. Yin, X. Lu, B. Sheng, S. Lu, “iFridge: an intelligent fridge for food management based on RFID technology” in *UbiComp '13 Adjunct: Proceedings of the 2013 ACM Conference on Pervasive and Ubiquitous Computing Adjunct Publication, Sept., 2013, pp291-294,* https://doi.org/10.1145/2494091.2494181.

41) A. Hachani, I. Barouni, Z. Ben Said and L. Amamou, "RFID Based Smart Fridge," *2016 8th IFIP International Conference on New Technologies, Mobility and Security (NTMS)*, 2016, pp. 1-4, doi: 10.1109/NTMS.2016.7792472.

42) A. D. Noutchet, “Novel User Centric RFID Fridge Design,” in *Computer and Information Science,* Canadian Center of Science and Education, 2013, vol. 6, no. 2., ISSN 1913-8989

43) M.G. Beasley, et al., “Causes, consequences and prevention of refrigeration fires in residential dwellings,” Fire Safety Journal, vol. 102, pp. 66-76, 2018, https://doi.org/10.1016/j.firesaf.2018.11.001.